Water Resources Research

RESEARCH ARTICLE
10.1029/2023WR034466

Special Section:
Advancing flood characterization, modeling, and communication

An Integrative Framework for Assessment of Urban Flood Response to Changing Climate

Lalit Pal[1,2,3], Siddharth Saksena[4], Sayan Dey[1], Venkatesh Merwade[1], and Chandra Shekhar Prasad Ojha[2]

[1]Lyles School of Civil Engineering, Purdue University, West Lafayette, IN, USA, [2]Department of Civil Engineering, Indian Institute of Technology Roorkee, Roorkee, India, [3]Now at Department of Civil and Environmental Engineering, Virginia Tech, Blacksburg, VA, USA, [4]Department of Civil and Environmental Engineering, Virginia Tech, Blacksburg, VA, USA

Abstract Increasing frequency of extreme rainfall induced catastrophic urban flood events in recent decades demands proactive efforts to assess flood risk and vulnerability. Here, we develop an integrative framework for fine spatiotemporal scale assessment of urban flood response to historical and future projected changes in extreme precipitation. The framework includes three main components—nonstationary modeling of historical extreme precipitation, modeling of future precipitation, and urban flood simulations. It also provides robust estimates of uncertainty in design precipitation from statistical modeling, multiple climate models and stochastic uncertainty, estimated using machine learning techniques. We demonstrate the proposed framework for White Oak Bayou watershed in Houston, Texas, US. Two-dimensional hydrologic-hydraulic Interconnected Channel and Pond Routing model is used to simulate flood response from design precipitation for historical (1986–2020) and two future (2021–2050 and 2071–2100) periods in three (SSP1-2.5, SSP2-4.5, and SSP5-8.5) future climate scenarios. Results show that nonstationary design estimates for historical precipitation are 14%–25% higher than the stationary estimates for 100-year event of 1- to 24-hr duration. Contrary to general global trends, we found a significant reduction in future design precipitation in all three emission scenarios. Additionally, stochastic uncertainty in future design precipitations is found to be larger than the modeling uncertainty in historical estimates and climate model uncertainty in future estimates. Flood response in terms of peak flood and total flood volume suggests that the difference in stationary versus nonstationary historical and future design precipitation are substantial to cause considerable change in simulated flood.

Plain Language Summary Global warming induced increase in extreme precipitation events has been the primary cause of frequent catastrophic floods in the recent decades—majorly impacting the urban agglomerations. Informed flood mitigation planning requires adequate consideration of these changes in extreme precipitation. So far, researchers have developed methodologies to model flood response to either the historical observed or future projected change in precipitation, but not for simultaneous consideration of both. Regional-scale evidence shows that the changes in historical observations can be inconsistent or sometimes contrasting to the changes in future projections from global climate models. Therefore, a collective assessment that includes the information of both historical and future changes in extreme precipitation is crucial. Here, we develop a comprehensive framework that incorporates both historical as well as future projected changes in extreme precipitation for fine spatiotemporal scale assessment of urban flood response. The framework also provides robust estimates of uncertainty from multiple components involved in the methodology which allows a reliable communication of attained information to stake holders and water resources planners for efficient decision making. The framework is independent of any regional assumption, thus can be used with confidence for other major cities of the world.

Key Points:

- A framework is proposed for fine-scale assessment of urban floods that incorporates historical as well as future changes in precipitation
- It also provides estimates of uncertainty from statistical modeling of extremes, multiple climate models, and stochastic uncertainty
- The framework is demonstrated for an urbanized watershed in Houston, Texas, United States to answer two important research questions

Supporting Information:

Supporting Information may be found in the online version of this article.

Correspondence to:

L. Pal,
lalitpl4@gmail.com

Citation:

Pal, L., Saksena, S., Dey, S., Merwade, V., & Ojha, C. S. P. (2023). An integrative framework for assessment of urban flood response to changing climate. *Water Resources Research*, *59*, e2023WR034466. https://doi.org/10.1029/2023WR034466

Received 10 JAN 2023
Accepted 9 AUG 2023

Author Contributions:

Conceptualization: Lalit Pal
Data curation: Lalit Pal
Formal analysis: Lalit Pal
Funding acquisition: Lalit Pal, Venkatesh Merwade, Chandra Shekhar Prasad Ojha

1. Introduction

Intense global warming over the last century has altered the precipitation patterns around the world, as explained by the Clausius-Clapeyron relationship (Allen & Ingram, 2002; IPCC, 2014; Trenberth et al., 2003). Extreme precipitation in particular exhibits a significant increase over large parts of the world in the last half century—largely attributed to anthropogenic climate warming (Alexander et al., 2006; Du et al., 2019; Fischer & Knutti, 2015; Westra et al., 2013). Though, there also exist considerable regional heterogeneity in extreme precipitation trends, driven by multiple factors including large-scale climate circulations, meso-scale weather systems (e.g., tropical cyclones), urbanization, aerosol concentration, and agricultural irrigation systems (Asadieh & Krakauer, 2015;

Investigation: Lalit Pal, Siddharth Saksena, Sayan Dey
Methodology: Lalit Pal, Siddharth Saksena, Sayan Dey, Venkatesh Merwade, Chandra Shekhar Prasad Ojha
Resources: Venkatesh Merwade
Software: Lalit Pal
Supervision: Venkatesh Merwade, Chandra Shekhar Prasad Ojha
Validation: Lalit Pal
Visualization: Lalit Pal
Writing – original draft: Lalit Pal
Writing – review & editing: Siddharth Saksena, Venkatesh Merwade, Chandra Shekhar Prasad Ojha

DeFlorio et al., 2013; Devanand et al., 2019; Kenyon & Hegerl, 2010; Sillmann et al., 2013; Singh et al., 2020; W. Zhang et al., 2018; X. Zhang et al., 2010; Zhao et al., 2019). Future climate simulations further provide a strong agreement on increased extreme precipitation in mid to late 21st century; significantly over parts of North America, Australia, South America, and Southeast Asia (Chou et al., 2009; Donat et al., 2013, 2016; Scoccimarro et al., 2013). The increasing trends in both historical and future extreme precipitation indicate an increasing risk of floods and associated losses, worldwide (Hallegatte et al., 2013; Hirabayashi et al., 2013; S. Sharma et al., 2021; Winsemius et al., 2016). Urban agglomerations are worst affected by the flood devastations due to high population density, poorly planned or outdated infrastructure, and changing climate (Berndtsson et al., 2019; Egger & Maurer, 2015; O'Donnell & Thorne, 2020; Yazdanfar & Sharma, 2015). Yet, existing standards for infrastructure design and flood management policies in most countries are defined with the assumption of a stationary climate. It constitutes a major challenge for engineers and water planners and highlights the need for adequate consideration of changes in extreme precipitation in infrastructure design and flood mitigation plans.

Several studies have reported a significant increase in extreme precipitation over the United States (US), both in historical observations and future projections from multiple climate models (Easterling et al., 2017; Groisman et al., 2001; Huang et al., 2018; Janssen et al., 2014; Reidmiller et al., 2017; Villarini et al., 2013; Vu & Mishra, 2019; Wright et al., 2019). A major consequence of the increase in extreme precipitation is observed as frequent devastating floods in different parts of the US that constituted about 43% of total natural hazards between 1995 and 2015, thus emerging as second deadliest and most costly natural disaster (Ashley & Ashley, 2008; Wallemacq et al., 2015). Multiple major cities of the US, particularly along the southern and eastern coastal plains have experienced frequent catastrophic floods in recent years, causing more than 25,000 fatalities in the last half century (Adhikari et al., 2010; Rappaport, 2014). The majority of these floods occurred from prolonged episodes of extreme precipitation from landfalling intense cyclonic activities (hurricanes and tropical storms) in the surrounding ocean (Kunkel et al., 2010; Villarini et al., 2014). Observational evidence suggests a rise in the frequency and intensity of tropical cyclones and associated extreme precipitation events, particularly in the Atlantic Ocean, in response to warming climate (Guzman & Jiang, 2021; IPCC, 2014; Van Oldenborgh et al., 2017; Webster et al., 2005). The future projections on overall frequency of tropical cyclones lacks confidence in the existing literature, though, there is a general agreement on potential increase in intense hurricanes and the intensity of extreme precipitation from tropical cyclonic activities (Knutson et al., 2010, 2013; Patricola & Wehner, 2018; Scoccimarro et al., 2014; Sobel et al., 2016; Van Oldenborgh et al., 2017; Wright et al., 2015).

Regardless of the observed and future projected increase in extreme precipitation, the existing design standards for urban infrastructure and flood mitigation strategies in the US are based on the assumption of stationary climate (L. Cheng & AghaKouchak, 2014; Das et al., 2013). For example, the design precipitation estimates provided by the National Oceanic and Atmospheric Administration (NOAA) in Atlas-14 are computed by considering stationary (i.e., no significant trends) extreme precipitation (Perica et al., 2018; Tousi et al., 2021; Underwood et al., 2020). Recent studies have challenged this assumption and demonstrated that the stationarity assumption considerably underestimate the design return levels in comparison to the nonstationarity based design precipitation for different parts of the US (L. Cheng & AghaKouchak, 2014; Vu & Mishra, 2019). In addition, flood inundation maps provided by the Federal Emergency Management Agency (FEMA) in the US also assume the time series of extreme streamflow to be stationary (Federal Emergency Management Agency (FEMA), 2022; S. Sharma et al., 2021; Villarini et al., 2009). Researchers have shown considerable differences in flood inundation maps of FEMA and the maps that account for nonstationarity (S. Sharma et al., 2021; Wing et al., 2018). Studies also report an increase in future projected flood magnitude and inundation under high emission climate scenario (Das et al., 2013). The increasing evidences of unprecedented extreme precipitation resulting in severe urban floods highlight the urgent need to factor the changing extreme precipitation patterns to re-evaluate existing infrastructure design and flood mitigation strategies for urban landscapes (Milly et al., 2008; Wing et al., 2018).

Literature contains multiple approaches to model extreme precipitation changes and their applications in estimation of design precipitation, flood frequency analysis, urban flood risk assessment, and attribution studies (Das et al., 2013; Karamouz et al., 2017; Kourtis & Tsihrintzis, 2021; Mattos et al., 2021; Padulano et al., 2021; S. Sharma et al., 2021; Tousi et al., 2021; Vemula et al., 2019). However, a close review reveals multiple gaps, particularly in the studies concerning urban flood response to changing climate. First, existing studies have either considered the historical changes or the future projected changes in their assessment, but not both. A reliable impact assessment, however, should include the changes in both observed and future projected precipitation. It is essential because extreme precipitation trends in future projections can be inconsistent, or sometimes in contrast

to that in the observations (Ban et al., 2021; Feng et al., 2021; Ridder et al., 2021; Wehner et al., 2015). Second, past studies on nonstationary modeling of historical extreme precipitation are limited to the estimation of nonstationary intensity-duration-frequency (IDF) curves. Therefore, an important question of how and to what extent the change in design precipitation will reflect in the urban flood response remains unanswered. The difference in simulated streamflow from nonstationarity versus stationary precipitation estimates can be insignificant owing to the inherent complexities of a fine-scale urban flood model (Padulano et al., 2021; S. Sharma et al., 2021). It is important to examine whether significant change in design precipitation from stationary versus nonstationary modeling translates to a significant change in simulated flood response.

Third, studies involving future climate change impact assessment on urban floods are performed at continental (Bates et al., 2021) and large watershed (C. Cheng et al., 2017; S. Sharma et al., 2021) scale. Large-scale analysis allows a direct use of general circulation model (GCM) outputs at native temporal resolution (i.e., daily time steps), only requiring spatial downscaling. However, the hydrologic response time in urban catchments is generally on the order of sub-daily to sub-hourly time scales, which requires simultaneous spatial and temporal downscaling of GCM outputs (Zahmatkesh et al., 2015). Multiple approaches are available in the literature for spatiotemporal downscaling of GCM precipitation yet there lacks a framework for their application in urban flood analysis. Fourth, researchers have proposed efficient methods to quantify uncertainty from different sources in a conventional urban flood modeling framework (Z. Liu & Merwade, 2018). However, there lacks a comprehensive methodology to estimate relative and combined uncertainty from additional uncertainty sources involved in modeling urban flood response to climate change such as, future projections from GCMs and spatiotemporal downscaling. A robust estimation of uncertainty in flood simulations is critical for reliable communication of flood hazards to stakeholder and decision makers (Collet et al., 2018; Sanders et al., 2020).

Here, we attempt to address these gaps and design a comprehensive framework for robust analysis of urban flood response to historical and future change in climate. The influence of climate change is introduced by considering changing patterns in extreme precipitation both in historical records and future projections. The novelty of the proposed framework lies in—(a) translation of modeled change in extreme precipitation to flood responses, (b) assimilation of stochastic weather generator based downscaling approach in urban flood assessment, (c) application of probabilistic machine learning based uncertainty estimation technique for future design precipitation and its representation in flood simulations. With the developed methodology, we attempt to address two important research questions: (a) Does climate change induced precipitation changes reflect in fine-scale urban flood simulations? and (b) Which source of uncertainty dominates the climate change driven flood simulations? We focus on understanding the influence of climate change induced changes in extreme precipitation on flood response in an urban environment. For the case study, we considered the watershed of White Oak Bayou in the city of Houston, Texas, USA. Houston has experienced several flood events in the recent past, including the most devastating floods from Hurricane Harvey in August 2017. The proposed framework will allow a comprehensive assessment of urban flood response with the consideration of changing extreme precipitation characteristics that would benefit in planning flood mitigation strategies and evaluate infrastructure safety in the region.

2. Study Area and Data

2.1. Study Area

To demonstrate the proposed framework, we selected the watershed of White Oak Bayou in Harris County of Texas, US (Figure 1). White Oak Bayou originates near Highway 6 and US Highway 290, traverse southeast to join Buffalo Bayou in downtown Houston. The watershed of White Oak Bayou covers an area of about 310 km^2, with relatively flat relief (~0.1%) and elevation range 0–49 m above mean sea level. According to National Land Cover Database land cover data for 2019, more than 96% of the watershed is developed land where about 60% of the area is impervious (Figure S1 in Supporting Information S2). Houston has historically experienced several catastrophic floods mainly caused by prolonged episodes of extreme rainfall brought by landfalling tropical cyclones in the Gulf of Mexico. The region shares a subtropical climate with hot and humid summers, and mild winters. Mean (minimum/maximum) temperature in summer (June-August) rises to 28.2°C (11.7°C/42.2°C) and drops to 11.6°C (−13°C/28.3°C) in winter (December-February). Relative humidity typically ranges between 70% and 75% throughout the year. The soil type in the region is loamy with high clay content that exhibits moderate to very slow drainage, shallow water table, and is classified in hydrologic soil group D. The longest flow path in the watershed is 48.7 km and the time of concentration estimated using Kirpich formula is 23.6 hr. The

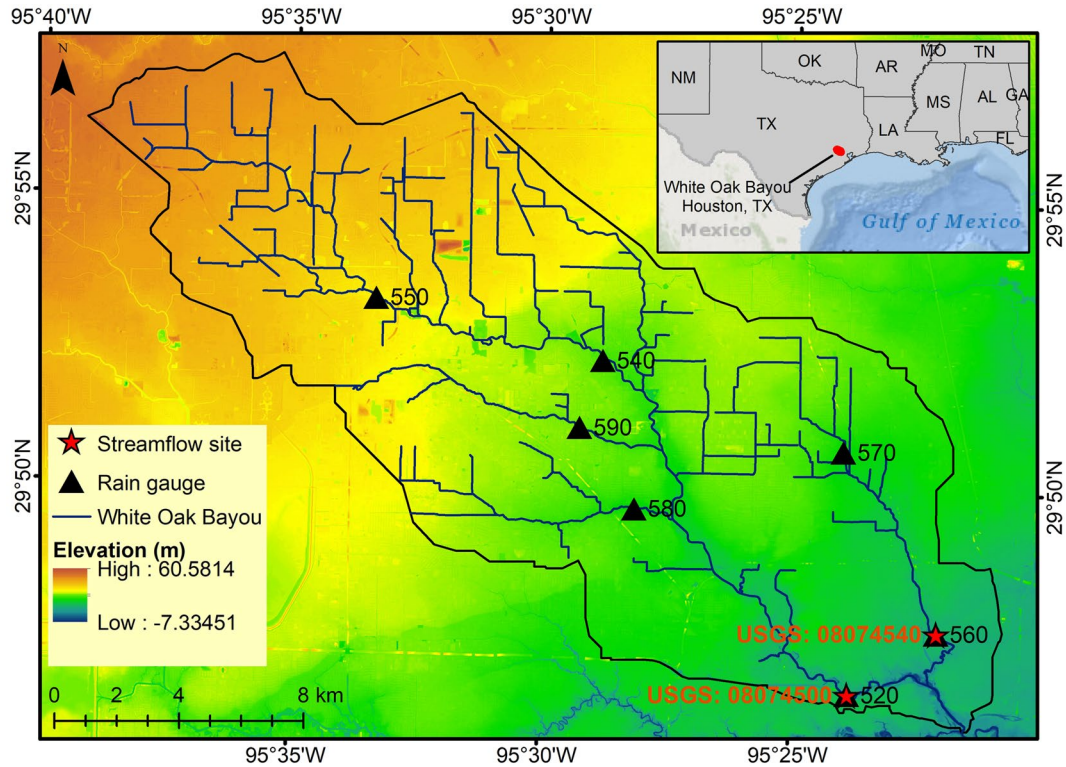

Figure 1. The watershed of White Oak Bayou in Harris County of Texas, US. Map shows the stream network of White Oak Bayou, location of rain gage stations, elevation range, and streamflow gauging sites in the watershed.

watershed is characterized by subtropical climate with cyclonic activities induced extreme precipitation events, extensive urbanization, and flatter topography. These attributes are common to several major cities of the world.

2.2. Data

In observational data set, we acquired precipitation data for White Oak Bayou from Harris County Flood Control District's Flood Warning System at 5-min intervals. Table 1 lists seven gauging stations selected for the study based on the availability of a long-term record covering 1986–2020. We obtained NOAA design precipitation estimates for station 520 designated as "Houston Heights" (Site ID: 41-4321). Observed streamflow record is obtained from the US Geological Survey National Water Information System for site 08074500 and 08074540 at 15-min interval (https://waterdata.usgs.gov/nwis). Meteorological variables used in the study are—air temperature, relative humidity, wind speed, atmospheric pressure, cloud cover, and shortwave solar radiation. Hourly data of all meteorological variables except for shortwave radiation are acquired from NOAA's Local Climatological

Table 1
Geographic Details of Rainfall Gauge Stations in White Oak Bayou Adopted for Present Study

ID	Rainfall gage (White Oak Bayou)	Latitude	Longitude	Elevation (m)
520	White Oak Bayou, Heights Boulevard	29.77488	−95.3971	12.27
540	White Oak Bayou, Alabonson Road	29.87042	−95.4804	23.6
550	White Oak Bayou, Lakeview Drive	29.88736	−95.5562	29.61
560	Little White Oak Bayou, Trimble Street	29.79296	−95.3678	14.18
570	Little White Oak Bayou, Tidwell Road	29.84514	−95.3997	19.55
580	Brickhouse Gully, Costa Rica Road	29.82766	−95.469	19.6
590	Cole Creek, Deihl Road	29.85089	−95.4877	24.35

Data (https://www.ncei.noaa.gov/products/land-based-station/local-climatological-data). We used the meteorological data from six weather stations surrounding the watershed—Houston Ellington, Intercontinental Airport, Houston William Hobby, Houston Dunn Helistop, Houston Clover Field, and Houston Hooks Memorial Airport. Solar radiation data set is downloaded from the archive of National Solar Radiation Database (https://nsrdb.nrel.gov/data-sets/archives). The fine resolution distributed hydrodynamic model used for flood simulation in this study is data intensive requiring multiple high-quality data sets. We integrate several public domain data sets to develop the model. In addition to rainfall and streamflow data set, we acquired impervious cover data in raster grid format from The USGS National Map Viewer portal (https://apps.nationalmap.gov/downloader/) for the year 2019. The information on soil properties and sub-surface layers is obtained from the National Resources Conservation Services Gridded Soil Survey Geographic Database for the year 2017.

The timeseries of Niño 3.4 sea surface temperature (SST) index used as an indicator of El Niño-Southern Oscillations (ENSO) phases is downloaded from NOAA Working Group on Surface Pressure (https://psl.noaa.gov/gcos_wgsp/Timeseries/). The global average surface temperature time series is obtained from NOAA Global Surface Temperature Dataset version 4.0 (https://data.giss.nasa.gov/gistemp/). We used Hadley Centre Sea Ice and SST data set (HadISST2) from Met Office Hadley Centre observations (https://www.metoffice.gov.uk/hadobs/hadisst2/) to obtain SST over the Tropical North Atlantic (TNA) Ocean. Time series of TNA SST is computed as area average SST over the domain 5°–25°N, 15°–55°W (Enfield et al., 1999). Each time series of global surface and sea surface temperatures is detrended prior to use in the analysis. Note that historical records of all the parameters are acquired for the period 1986–2020 designated as "historical" period. The historical period of 1986–2020 is selected based on the availability of long-term observed precipitation data for rain gauges located in the watershed.

Daily realizations of GCMs available under Coupled Model Intercomparison Project Phase 6 (CMIP6) are used to obtain future projections of precipitation and temperature (https://esgf-node.llnl.gov/projects/cmip6/). We chose a total of 15 GCMs based on their performance reported in the literature (Agel & Barlow, 2020; Srivastava et al., 2020) (Table S1 in Supporting Information S3). In CMIP6 project, GCM simulations with historical forcings are available for the period 1850–2014, therefore, we used GCM's historical outputs for the period 1986–2014 designated as "control" period in the study. GCM's future projections are acquired for two 30-year future periods, 2021–2050 and 2071–2100 representing "near future" and "far future", respectively. For this study we strategically selected three future emission scenarios used in CMIP6 project called "Shared Socioeconomic Pathways" (SSPs)—SSP1-2.6 denoting sustainable future with controlled GHG emissions, SSP2-4.5 denoting moderate reduction in GHG emissions with intermediate mitigation and adaptation, and SSP5-8.5 denoting very high GHG emissions with low mitigation (Riahi et al., 2017).

3. Methodology

Figure 2 illustrates the flow chart of proposed framework to investigate urban flood response in changing climate. The framework broadly consists of three main components—modeling of changes in historical extreme precipitation, modeling of extreme precipitation in future projections, and urban flood simulation for historical and future design precipitation. Extreme precipitation series are obtained as the annual maximum values of accumulated precipitation over different durations (5 min, 10 min, 15 min, 30 min, 1-hr, 2-hr, 3-hr, 6-hr, 12-hr, 24-hr, 2-day, 3-day, 4-day, 7-day, and 10-day). In the first step, historical time series of extreme precipitation for selected durations are tested for trend and stationarity at 5% significance level. Extreme precipitation series with statistically significant trend or nonstationary is modeled using nonstationary extreme value distribution, else stationary model is used. The extreme value distribution is used to obtain design precipitation for return period of 5, 10, 25, 50, 100, 200, 500, and 1,000 years to develop corresponding IDF curves. The uncertainty bounds on IDF curves are defined by computing confidence interval on design precipitation estimates using non-parametric bootstrap method at 95% confidence level (Gilleland, 2020).

Second, future projections of precipitation from selected GCMs are downscaled from daily to hourly time step for each station in the watershed using a stochastic downscaling approach described in Kim et al. (2016), Fatichi et al. (2013), and Fatichi et al. (2011). The approach utilizes delta change method in conjunction with a stochastic weather generator, Advanced WEather GENerator (AWE-GEN) (Fatichi et al., 2011; Ivanov et al., 2007) to simulate hourly precipitation for future period. The procedure also includes a probabilistic machine learning based technique called Bayesian Weighted Averaging (BWA) to estimate uncertainty from multiple GCMs

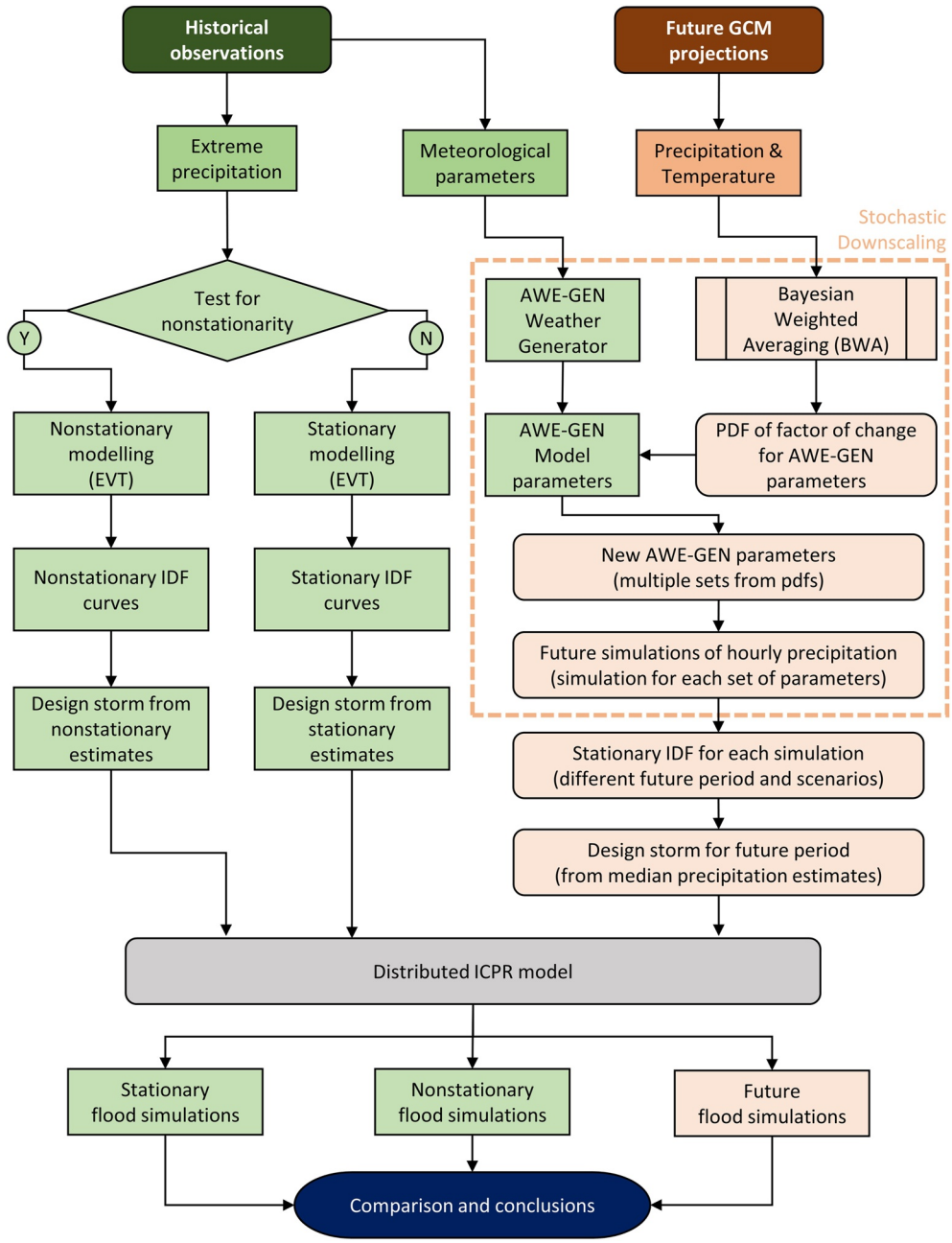

Figure 2. Flowchart of proposed framework to evaluate urban flood response in changing climate.

in downscaled future projections (Tebaldi et al., 2005). The stepwise downscaling procedure is described in Section 3.4. The procedure generates an ensemble of downscaled hourly time series of precipitation for two future time periods (2021–2050 and 2071–2100) using projections for three climate scenarios (SSP1-2.6, SSP2-4.5, and SSP5-8.5). Each precipitation time series in the ensemble of downscaled future projections is modeled using stationarity approach, and design precipitation estimates are derived for selected return periods. The process gives a set of design estimates for each return period, in which the median value is used to develop IDF curves for future periods and 95% quantile bounds of the distribution of estimates define the uncertainty limits of IDF curves. Using this procedure, future IDF curves are developed for each rainfall station in White Oak Bayou watershed.

Lastly, we used IDF curves of historical and future periods to create design storm for 100-year 24-hr event. Flood response corresponding to selected design storm is simulated using distributed Interconnected Channel and Pond

Routing (ICPR) urban flood model developed for White Oak Bayou. Simulated flood response from stationary design storm is compared with the historical nonstationary and future design storms in terms of peak flow and total flood volume. A detailed description of different components in the methodology is given in the following sections.

3.1. Test for Trend and Nonstationarity

Non-parametric Mann-Kendall (MK) test (Kendall, 1970; Mann, 1945) is used to detect monotonic trend in the time series of extreme precipitation at 5% significance level. Serially correlated series are tested using modified version of MK test proposed by Hamed and Ramachandra Rao (1998). Besides long-term trends, nonstationarity in extreme precipitation is tested using three commonly used methods—Augmented Dickey Fuller (ADF) test (Dickey & Fuller, 1979; Said & Dickey, 1984), Phillips-Perron (PP) test (Phillips & Perron, 1988), and Kwiatkwoski-Phillips-Schmidt-Shin (KPSS) test (Kwiatkowski et al., 1992). ADF and PP test are unit root tests with the null hypothesis of a unit root (difference stationarity) process against trend stationarity. Conversely, the null hypothesis of KPSS test assumes stationarity around a deterministic trend. KPSS test is used to validate the results of ADF and PP test as unit root-based tests show low power against stationarity near unit root processes (Dritsakis, 2004; Ganguli & Coulibaly, 2017). For time series to be strictly trend stationary, the null hypothesis of ADF and PP test should be rejected and null hypothesis of KPSS test should be accepted at 5% significance level. It is advised to log-transform the time series before applying the nonstationarity tests (Gimeno et al., 1999).

3.2. Statistical Modeling of Extreme Precipitation

We used the methods defined in extreme value theory to model extreme precipitation. In stationary modeling, extreme precipitation defined as annual maximum series is modeled using the generalized extreme value (GEV) distribution that describes the theoretical asymptotic distribution of block maxima (Coles, 2001). Van Der Wiel et al. (2017) from a detailed analysis, report that heavy tail distribution of extreme precipitation in US Gulf coast region is well described by GEV distribution. The mathematical description of GEV distribution and its parameter estimation is given in Appendix A.

In a widely adopted approach, nonstationarity is introduced by defining the parameters of selected extreme value distribution as a function of covariates of the modeled variable. We define nonstationary GEV model by scaling its location (μ) parameter as a linear function of covariates, while scale and shape parameters are kept constant. Potential covariates of extreme precipitation over southern coasts of the US considered in the study are—global mean temperature (tas) motivated by the Clausius–Clapeyron relationship, ENSO for large scale teleconnections, TNA SST as forcings to tropical cyclonic activities in the North Atlantic Ocean at synoptic to meso-scale, local air temperature (T_a) as forcings to local weather patterns, and time (t) as a measure of trends in extreme precipitation. Subsequently, candidate nonstationary GEV models are defined by scaling location parameter with the selected covariates, individually and in combinations. The list of all candidate GEV (stationary and nonstationary) models is given in Table 2.

The best-fit nonstationary GEV model is identified using three commonly used criteria—Akaike Information Criteria (AIC), Bayesian Information Criteria (BIC), and Likelihood Ratio (LR) test (Appendix A). Multiple past studies have used these criteria for the selection of best-fit nonstationary extreme value distribution (Katz, 2013; Mondal & Mujumdar, 2015). The best-fit nonstationary GEV model is used to estimate design precipitation for selected return periods. The confidence interval on the design estimates (for both stationary and nonstationary models) is estimated using non-parametric bootstrap resampling method explained by Gilleland (2020). In the procedure, non-parametric resampling is performed on the fitted GEV distribution to obtain sampled set of extremes for making statistical inference. Statistical modeling of extreme precipitation and estimation of bootstrap-based confidence interval on design precipitation is performed using the R package "extRemes" v2.1-1 developed by (Gilleland & Katz, 2016).

3.3. Development of IDF Curves and Design Storm

The model (stationary or nonstationary) parameter estimates are used to compute the design precipitation intensity (or return level) for a given probability of exceedance, p. The probability of exceedance (p) is linked to the

Table 2
Description of Candidate Stationary and Nonstationary Generalized Extreme Value (GEV) Model Structure Adopted in the Study

S. no.	Description	S. no.	Description
1	$X \sim \text{GEV}(\mu,\sigma,\xi)$	9	$X \sim \text{GEV}(\mu_0 + \mu_1.t + \mu_2.\text{TNA},\sigma,\xi)$
2	$X \sim \text{GEV}(\mu_0 + \mu_1.t,\sigma,\xi)$	10	$X \sim \text{GEV}(\mu_0 + \mu_1.t + \mu_2.T_a,\sigma,\xi)$
3	$X \sim \text{GEV}(\mu_0 + \mu_1.\text{ENSO},\sigma,\xi)$	11	$X \sim \text{GEV}(\mu_0 + \mu_1.\text{tas} + \mu_2.\text{ENSO},\sigma,\xi)$
4	$X \sim \text{GEV}(\mu_0 + \mu_1.T_a,\sigma,\xi)$	12	$X \sim \text{GEV}(\mu_0 + \mu_1.\text{tas} + \mu_2.\text{TNA},\sigma,\xi)$
5	$X \sim \text{GEV}(\mu_0 + \mu_1.\text{tas},\sigma,\xi)$	13	$X \sim \text{GEV}(\mu_0 + \mu_1.\text{tas} + \mu_2.T_a,\sigma,\xi)$
6	$X \sim \text{GEV}(\mu_0 + \mu_1.\text{TNA},\sigma,\xi)$	14	$X \sim \text{GEV}(\mu_0 + \mu_1.\text{ENSO} + \mu_2.\text{TNA},\sigma,\xi)$
7	$X \sim \text{GEV}(\mu_0 + \mu_1.t + \mu_2.\text{tas},\sigma,\xi)$	15	$X \sim \text{GEV}(\mu_0 + \mu_1.\text{ENSO} + \mu_2.T_a,\sigma,\xi)$
8	$X \sim \text{GEV}(\mu_0 + \mu_1.t + \mu_2.\text{ENSO},\sigma,\xi)$	16	$X \sim \text{GEV}(\mu_0 + \mu_1.\text{TNA} + \mu_2.T_a,\sigma,\xi)$

return period (T) of a rainfall event as $T = 1/p$. In other words, "T" year rainfall event represents the intensity of annual maximum rainfall of a given duration that has $1/T$ probability of exceeding in a given year (L. Cheng & AghaKouchak, 2014). Design storm for a given duration and return period is developed using alternate block method (Chow et al., 1988).

3.4. Downscaling of Future Precipitation

In the first step, we selected the best five out of 15 initially chosen GCMs by evaluating historical simulations of GCMs against the observed precipitation for extreme precipitation characteristics (see Appendix A). In this study, we performed point-scale stochastic downscaling of precipitation using an hourly stochastic weather generator, AWE-GEN (Fatichi et al., 2011; Ivanov et al., 2007). AWE-GEN is capable of reproducing key meteorological variables, including, precipitation, air temperature, wind speed, cloud cover, incoming shortwave radiation, and atmospheric pressure at hourly time scale for a given location. AWE-GEN model setup generates a set of statistics called model parameters, describing the stochastic and statistical properties of the modeled meteorological variables. Past applications of AWE-GEN demonstrate its competence to simulate low and high-frequency components of hydrometeorological variables, the inter-annual variability, and extreme characteristics of precipitation (Fatichi et al., 2011; Ivanov et al., 2007; Kim et al., 2016). A detailed description of AWE-GEN model structure and working can be found in Fatichi et al. (2011) and Ivanov et al. (2007). A MATLAB package for AWE-GEN is available as open source at the repository of ETH Zürich (https://hyd.ifu.ethz.ch/research-data-models/awe-gen.html) and University of Michigan (http://www-personal.umich.edu/~ivanov/HYDROWIT/Models.html).

A detailed description of stochastic downscaling procedure using AWE-GEN model is provided in Fatichi et al. (2011, 2013), and Kim et al. (2016). Following paragraphs briefly explain the steps involved in the procedure.

- The set of statistics generated in AWE-GEN model setup are also computed from GCM simulations for control and future periods, separately for each GCM. The statistics for precipitation include mean, variance, skewness, and frequency of no precipitation, computed for multiple aggregation interval (i.e., 24, 48, 72, and 96 hr) for each month. Temperature statistics include the monthly mean values.
- The uncertainty in future projections from multiple GCMs is estimated using BWA approach (R. L. Smith et al., 2009; Tebaldi et al., 2005) that assigns weights to the realization of different GCMs. Model weights are defined based on—(a) "bias" with respect to historical observations (model performance in current climate), and (b) "convergence" among model realizations for future climate (deviation of model simulation from the central tendency of the ensemble). The objective of the procedure is to obtain posterior probability distribution for parameters of a five-parameter Bayesian statistical model—true mean value of hydrometeorological variables for control and future period (μ, ν), correlation coefficient between current and future projections (β), "precision" parameter defined as inverse of variance for simulation from the members of GCM ensemble (λ_i, where i is ensemble member), and a parameter that accounts for the "precision" of future simulations against historical observation (θ). A detailed description of Bayesian model setup is provided in Tebaldi et al. (2005) and its application to stochastic downscaling is explained by Fatichi et al. (2013) and Kim et al. (2016). The posterior distribution of Bayesian model parameters is numerically simulated using Markov Chain Monte

Carlo (MCMC) technique. In MCMC simulation procedure, we choose a burn-in period of 25,000 iterations to ensure independent and identically distributed sample of parameters, and a sampling interval of 50 iterations. The posterior distribution for each model parameter is defined with 1,000 sampled points estimated from a total of 75,000 iterations. The procedure is used to estimate posterior distribution of AWE-GEN model parameters for control and future period.

- Each set of simulated parameters (μ, ν) representing the true value of variable for control and future climate is used to compute factor of change (FC) for 170 distinct statistics of temperature and precipitation used in AWE-GEN. Product FCs are applicable to the statistics of precipitation, computed as the ratio of value of statistics for future and control period. Additive FCs are applicable to the statistics of temperature, computed as the difference of statistics between future and control period.

$$\text{Product FC} = \frac{S(h)^{\text{GCM,FUT}}}{S(h)^{\text{GCM,CT}}} \tag{1}$$

$$\text{Additive FC} = \left(T_{\text{mon}}^{\text{GCM,FUT}} - T_{\text{mon}}^{\text{GCM,CT}}\right) \tag{2}$$

- For computational efficiency, we sample 51 sets of FCs from the posterior pdfs using Sobol quasi-random low discrepancy sequence (Saltelli et al., 2009; Sobol, 1976). One in 51 sets of FCs is obtained from the median of posterior pdfs that corresponds to the median future trajectory. Each sampled set of FCs is applied to the AWE-GEN model parameters derived from historical observations to get a new set of model parameters representing a trajectory in future climate. For each set of model parameters, 50 simulations are performed to describe stochastic uncertainty in model simulations. Thus, we performed a total of 2,550 (51 trajectories × 50 simulations) simulations for a given future period in a given scenario at each station that capture stochastic and climate model uncertainties in future downscaled hourly time series of precipitation.

3.5. Partitioning of Uncertainties in Future Precipitation

Ensemble of AWE-GEN model simulations are used to partition uncertainty in design precipitation from two main sources—climate models (multiple GCMs) and stochastic (climate internal variability) uncertainty, considering the sources to be dependent by accounting for the co-variance among uncertainty sources (Fatichi et al., 2016). The uncertainties are partitioned for two future periods and three emission scenarios. To estimate climate model uncertainty, for a given duration and return period, we take the median of design precipitation from 50 stochastic simulation of AWE-GEN for all 51 future climate trajectories. We compute the difference in 5th and 95th percentiles of the 51 median values corresponding to a future climate trajectory and take the average of 5–95th percentile ranges for three emission scenarios. To compute the stochastic uncertainty, we compute the 5–95th percentile range from 50 stochastic simulations for median future trajectory and take the average of percentile ranges for three emission scenarios. Total uncertainty in future design precipitation is computed as the 5–95th percentile range estimated from all 2,550 simulations (51 future trajectories × 50 stochastic simulations). Note that the total uncertainty computed here will not amount to the sum of climate model and stochastic uncertainty due to their mutual overlap as the two sources are not considered to be independent. Accordingly, the computed uncertainty magnitudes are normalized by the total uncertainty to quantify their fractional contribution.

3.6. Hydrodynamic Model Description

The goal of urban flood modeling in this study is to investigate the flood response of selected urbanized watershed to design extreme precipitation obtained with and without the consideration of changing climate. We use physically based distributed ICPR approved by FEMA (Ahmad et al., 2014; Joyce et al., 2018; Saksena et al., 2019; Streamline Technologies, 2016, 2018). ICPR allows the application of variable surface roughness for shallow and deep overland flow. During large flood events, the roughness changes over time when the depth of the water in the floodplain increases due to persistent flooding. Popular hydraulic models such as the Hydrologic Engineering Center's River Analysis System (HEC-RAS) and LISFLOOD-FP, do not account for this variability (Bates & De Roo, 2000; Brunner, 2016). Saksena et al. (2020) developed a detailed ICPR model for a portion of Harris County covering several watersheds including the San Jacinto River Basin and the Buffalo Bayou that also encompassed the watershed of White Oak Bayou. In that study, ICPR model was developed with

Table 3
Trend and Stationarity Test Results for Annual Maximum Series of 24-Hour Precipitation at Seven Stations in White Oak Bayou, Houston, Texas

	MK test		Sen's slope	ADF	PP	KPSS
Station	Z-value	p-value	β (mm/year)	p-value	p-value	p-value
520	2.102	0.036	1.588	0.056	0.010	0.072
540	9.949	0.000	1.869	0.224	0.010	0.100
550	3.281	0.001	2.642	0.016	0.010	0.100
560	2.172	0.030	1.626	0.010	0.010	0.100
570	3.494	0.001	2.609	0.012	0.010	0.081
580	4.222	0.000	2.339	0.016	0.010	0.100
590	2.743	0.006	2.078	0.010	0.010	0.100

Note. The null hypothesis of trend and stationarity test is rejected for p-value less than 0.05 at 5% significance.

two configurations—"small" model with fine spatial resolution and smaller hydraulic time steps and "large" model with coarser resolution and lager hydraulic time steps. For the present study, we use a subset of previously developed ICPR model for White Oak Bayou watershed with "small" model configuration. Reader is requested to refer to Saksena et al. (2020) for the detailed information on the model structure, setup and performance. Here, we briefly summarize the important information on the model configuration and setup.

Watershed boundaries and integrated network of natural and artificial channels in the watershed for White Oak Bayou are obtained from USGS's National Hydrology Database and NHDPlus High resolution data set of catchments and stream networks (Figure 1). We adopted a two-dimensional (2-D) model structure of ICPR that is simplified to include only the diffusive wave components of the full St. Venant equation to achieve higher computational efficiency. For more information on 1-D 2-D flow dynamics in ICPR, please refer to Saksena et al. (2020). The soil moisture is accounted for by including up to two of the three "vertical layers" defined to discretize the vadose zone, where third layer is assumed to be impervious, thus no water is lost from the system. Although, the dynamics of saturated aquifer can be modeled in ICPR by including a dynamic water table using groundwater module of ICPR model (Streamline Technologies, 2018). The maximum available water for subsurface layers above the third (impervious) layer is fixed based on the soil classes. We also employed the adaptive multiresolution scheme with local time stepping referred to as "FIREBALL" used by Saksena et al. (2020) that results in a significant reduction in runtimes. Since this study is focused on examining the relative response of the watershed for change in design precipitation, the initial hydrologic parameters of the model are not calibrated to reduce modeling efforts. The model simulations in term of streamflow are generated at half-hourly time steps for both historical and future design storms. The flood response is evaluated by comparing the simulated streamflow corresponding to 24-hr 100-year design storm generated from nonstationary IDF curves for historical period and future IDF curves for three scenarios and two future periods. Detailed mathematical formulations of different components of ICPR model can be found in Saksena et al. (2020) and Streamline Technologies (2018).

4. Results

4.1. Trend and Stationarity Test

Table 3 summarizes the results of trend and stationarity test for 24-hr extreme precipitation at each station in White Oak Bayou. Results show statistically significant increasing trend in extreme precipitation at all stations. The rate of increase in 24-hr extreme precipitation at different stations lies in the range 15.9–26.4 mm per decade, as obtained from Sen's slope values. The extreme precipitation series are also tested for higher order (unit root) nonstationarity using specialized statistical tests. Due to the presence of significant trends, unit root nonstationarity is tested around a deterministic trend using ADF, PP, and KPSS test. Results show that the annual maximum series at all seven stations is stationary around a deterministic trend at 5% significance level (Table 3). ADF and PP test reject the null hypothesis of unit root autoregressive nonstationarity at all the stations except for station 520 and 540 in ADF test. In addition, the KPSS test fails to the reject the null hypothesis of trend stationarity in all the series. Extreme precipitation series of 1-hr duration and above exhibit significant increase at most stations, while sub-hourly series show statistically insignificant increase (Tables S3–S9 in Supporting Information S3). In contrast, extreme precipitation of 5-min duration at most stations show declining trend but statistically insignificant. Overall, the results reveal statistically significant increase in extreme precipitation at all stations, however, higher order unit root process based nonstationarity is statistically insignificant for most durations (Table S3–S9 in Supporting Information S3). Nonetheless, the nonstationarity in the form of significant trend in extreme precipitation is accounted in statistical modeling of extremes.

4.2. Stationarity Based Design Precipitation Estimates

In compliance with NOAA Atlas 14, design precipitation estimates in the form of IDF curves are estimated assuming the annual maximum series of precipitation to be stationary (i.e., no trend). Stationarity based IDF curves form the basis for comparison with nonstationary and future design precipitation, and their corresponding

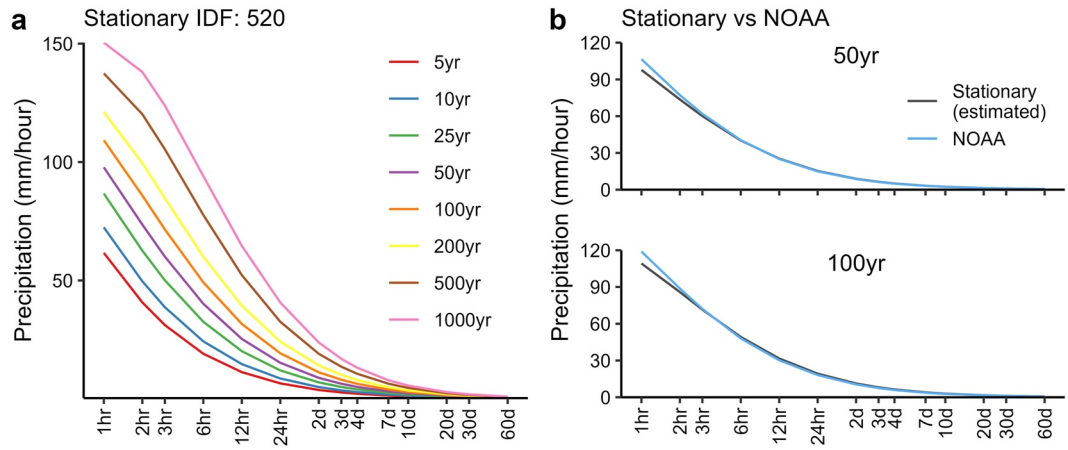

Figure 3. Estimated stationary intensity-duration-frequency (IDF) curves for station 520 in White Oak Bayou watershed and their comparison with National Oceanic and Atmospheric Administration (NOAA) based IDF curves for 50- and 100-year return period. (a) Stationarity-based IDF curves for station 520 in White Oak Bayou watershed. (b) Comparison of estimated stationary IDF and NOAA's IDF curves for 50-year and 100-year return period.

flood simulations. Note that results from most of the analyses in the study are similar for all stations in White Oak Bayou watershed. Therefore, we have shown the results for station 520 for brevity, unless mentioned otherwise. Figure 3 shows the stationary IDF curves developed for station 520 and their comparison with NOAA IDF curve for 50- and 100-year return period. The region receives substantial precipitation from extreme events as 10-year 1-hr design precipitation amounts to 50 mm, which rises to about 150 mm for a 100-year event. As evident from the comparison, estimated stationary design precipitation is fairly consistent with the NOAA estimates in which minor differences for short duration events can be due to the difference in period of analysis. The stationary IDF curves for all seven stations are provided in Figures S2–S8 in Supporting Information S2.

4.3. Nonstationarity Based Design Precipitation Estimates

An important step in nonstationary-based modeling of extremes is to identify potential large-scale or local physical drivers of observed changes to use as covariates. A preliminary correlation-based analysis between covariates and extreme precipitation of selected durations gives higher value of Spearman rank correlation for global average temperature (tas), suggesting its relatively higher potential for covariate in nonstationary model (Figure S9 in Supporting Information S2). However, a combination of more than one covariate can provide better model-fit to nonstationary extremes. Nonetheless, we performed a robust evaluation of candidate nonstationary GEV distributions based on AIC/BIC values and statistical significance in LR test. Figure 4 shows the rank of AIC/BIC values arranged in ascending order and statistical significance of LR test results for candidate models fitted to 24-hr extreme precipitation for all the stations. Extended results for all selected durations are provided in Figures S10–S12 in Supporting Information S2. As evident from Figure 4a, candidate GEV model with tas as covariate gives minimum value of AIC and BIC for majority of stations. Also, LR test results between nonstationary candidate model and stationary model are statistically significant for tas at all seven stations (Figure 4b). We obtained similar results for extreme precipitation of other durations with exceptions for a few durations at station 520 and 570 (Figures S10–S11 in Supporting Information S2). At these stations, combination of tas and ENSO gives best-fit model and tas only model gives the second best fit. Considering the applicability to majority of stations and to maintain consistency, candidate model with tas as covariate is adopted as best-fit nonstationary GEV model for further analyses.

Using the nonstationary GEV model with location parameter scaled on tas, we developed nonstationary IDF curves for all seven stations in the White Oak Bayou watershed. We obtained design precipitation using fitted nonstationary model corresponding to the value of covariate in the year 2020. Figure 5 shows the nonstationary IDF curves for station 520 and their comparison with stationary IDF curves for selected return periods. This figure also represents 95% uncertainty bounds of design precipitation computed using non-parametric bootstrap resampling. Evidently, stationarity-based design precipitation intensity for a given duration is considerably less than the nonstationarity-based estimates for all return periods. For instance, for 100-year 1-hr event at station 520, nonstationary (127 mm/hr) design precipitation is about 13.4% higher than the stationary (112 mm/hr) design

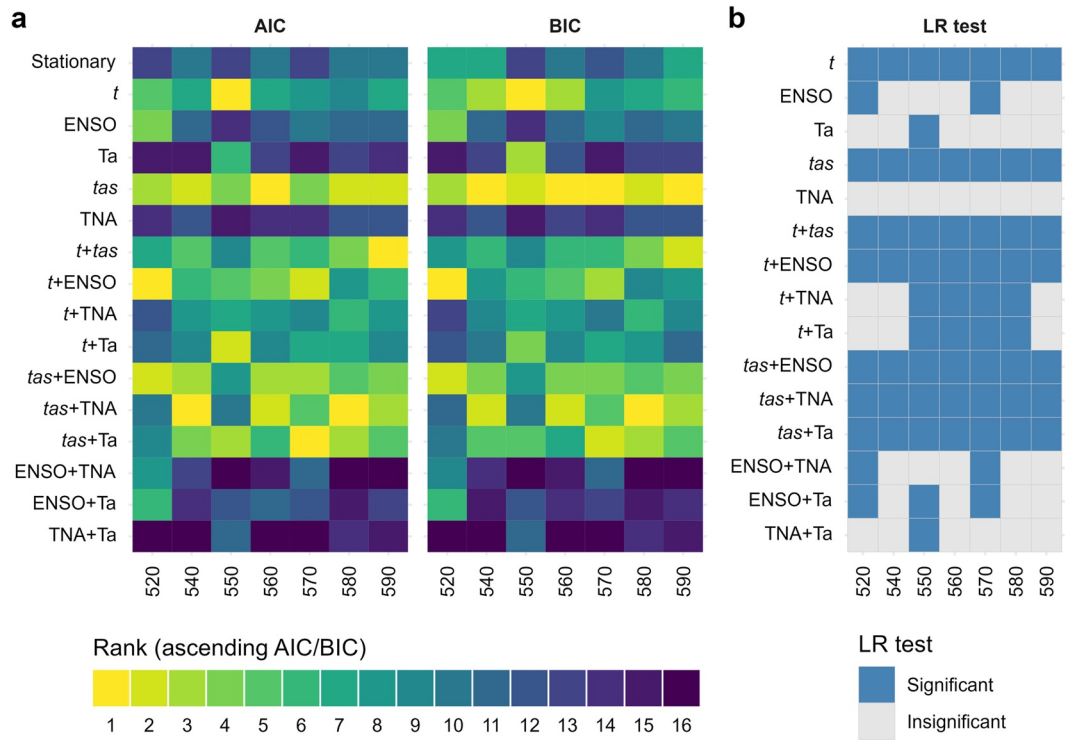

Figure 4. Evaluation of candidate nonstationary generalized extreme value (GEV) model for best-fit to 24-hr extreme precipitation at seven stations in White Oak Bayou watershed. (a) Rank of Akaike Information Criteria (AIC) and Bayesian Information Criteria (BIC) values arranged in ascending order for candidate nonstationary GEV model. (b) Statistical significance of candidate nonstationary GEV models versus stationary GEV model obtained from Likelihood Ratio (LR) test.

precipitation; while for 10-year 24-hr event, nonstationary (17 mm/hr) precipitation is about 19.8% higher than stationary (14 mm/hr) precipitation. Similar results are obtained at all seven stations in the watershed, except for station 550 where the difference between nonstationary and stationary estimates is relatively small (Figures S2–S8 in Supporting Information S2). Further examination shows that smaller difference at station 550 is evident for short (1- to 6-hr) durations (Figure S13 in Supporting Information S2). It can be due to inconsistent performance of selected covariates for time series of different duration. For urban watersheds that are typically characterized with quick hydrologic response, a 13%–20% increase in precipitation intensity can cause substantial increase in peak flood and consequent flood inundation. Accordingly, the actual risk of floods and its associated impact on infrastructure and services in this region can be much higher compared to estimates with stationary assumption. Also, flood mitigation measures designed on stationarity assumption can be under potential risk of failure. Note that for all durations, the difference in nonstationary and stationary estimates decreases for higher return period events, such that the difference is negligible for 1,000-year return period events. It is possibly due to the relatively short length of record (35 years) used in this study, whereby estimates for longer (500- and 1,000-year) return period involve considerable extrapolation with fitted GEV model that diminishes the effect of nonstationarity. The short length record is also responsible for substantially large uncertainty range for design precipitation of longer return periods.

Furthermore, the relative increase in design precipitation from nonstationary versus stationary modeling is higher for longer duration events and lower for short durations at all stations (Figure S13 in Supporting Information S2). It suggests that the longer duration extreme events have experienced larger changes than the short duration events in the historical period.

4.4. Future Design Precipitation Estimates

4.4.1. AWE-GEN Model Setup

AWE-GEN model is set up individually for all seven stations in the White Oak Bayou watershed for the historical (1986–2020) period. Due to the unavailability of weather station in the watershed, hourly time series of

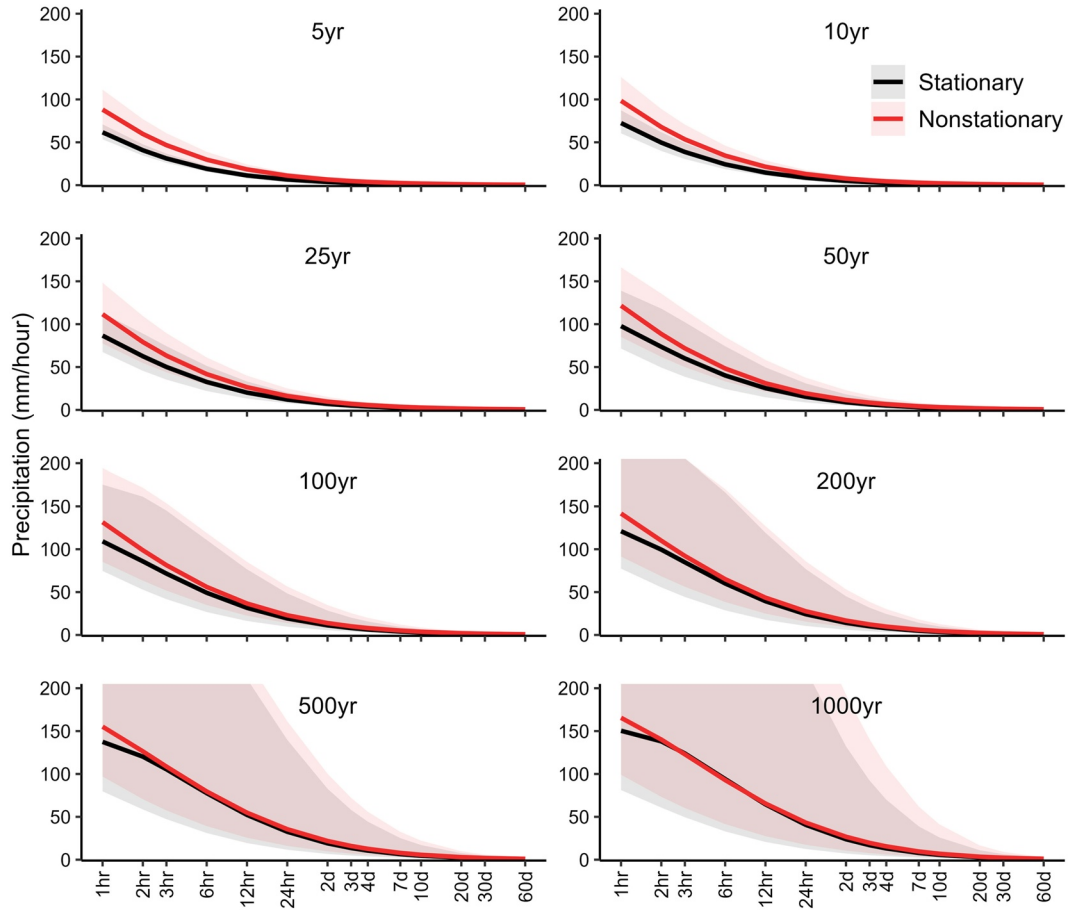

Figure 5. Comparison of nonstationary and stationary intensity-duration-frequency (IDF) curves for different return periods at station 520. Nonstationary IDF curves are developed using nonstationary generalized extreme value distribution with location parameter scaled on global average temperature (tas). Shaded region denotes 95% uncertainty bound of design precipitation computed using non-parametric bootstrap method.

meteorological variables required for model setup is obtained by interpolating from six surrounding weather stations using partial thin plate spline (PTPS) interpolation technique (Hutchinson & Gessler, 1994). PTPS is a commonly used technique for spatial interpolation of meteorological variables due to its computational efficiency and robust detection of error (Hofstra et al., 2008; Szentimrey et al., 2007). In case of missing values at three or more weather stations, the value at the closest station is adopted.

A comparison of observed and AWE-GEN simulated mean monthly precipitation and 24-hr extreme precipitation of different return periods is shown in Figure 6. Evidently, AWE-GEN model shows remarkable performance in reproducing mean monthly precipitation at all stations. Monthly precipitation from observations practically overlaps with the median of 50 stochastic simulations from AWE-GEN for all months. AWE-GEN model simulations give a narrow range of stochastic uncertainty for all months that reflects the model's potential in simulating historical observations in the study region. The model also performs satisfactorily in the simulation of extreme precipitation. Extreme precipitation estimates from observations are close to the median of extremes from model's stochastic simulations up to 15- to 20-year return period at different stations. For longer return periods, the extreme precipitation from observations deviates from the median value but falls well within the stochastic uncertainty limits of simulated precipitation. Further examination shows that the model performance in simulating extreme precipitation considerably improves when 2017 (the year when Hurricane Harvey occurred) is not considered. The Neyman-Scott Rectangular pulse process used in AWE-GEN exhibit limited capability in simulating low frequency variances (Fatichi et al., 2011). Thus, the deviations in simulated extreme precipitation for higher return period is probably due to unprecedented precipitation received from Hurricane Harvey in August 2017 (return period exceeding 1,000-year). Its effect on model performance can also be seen in the

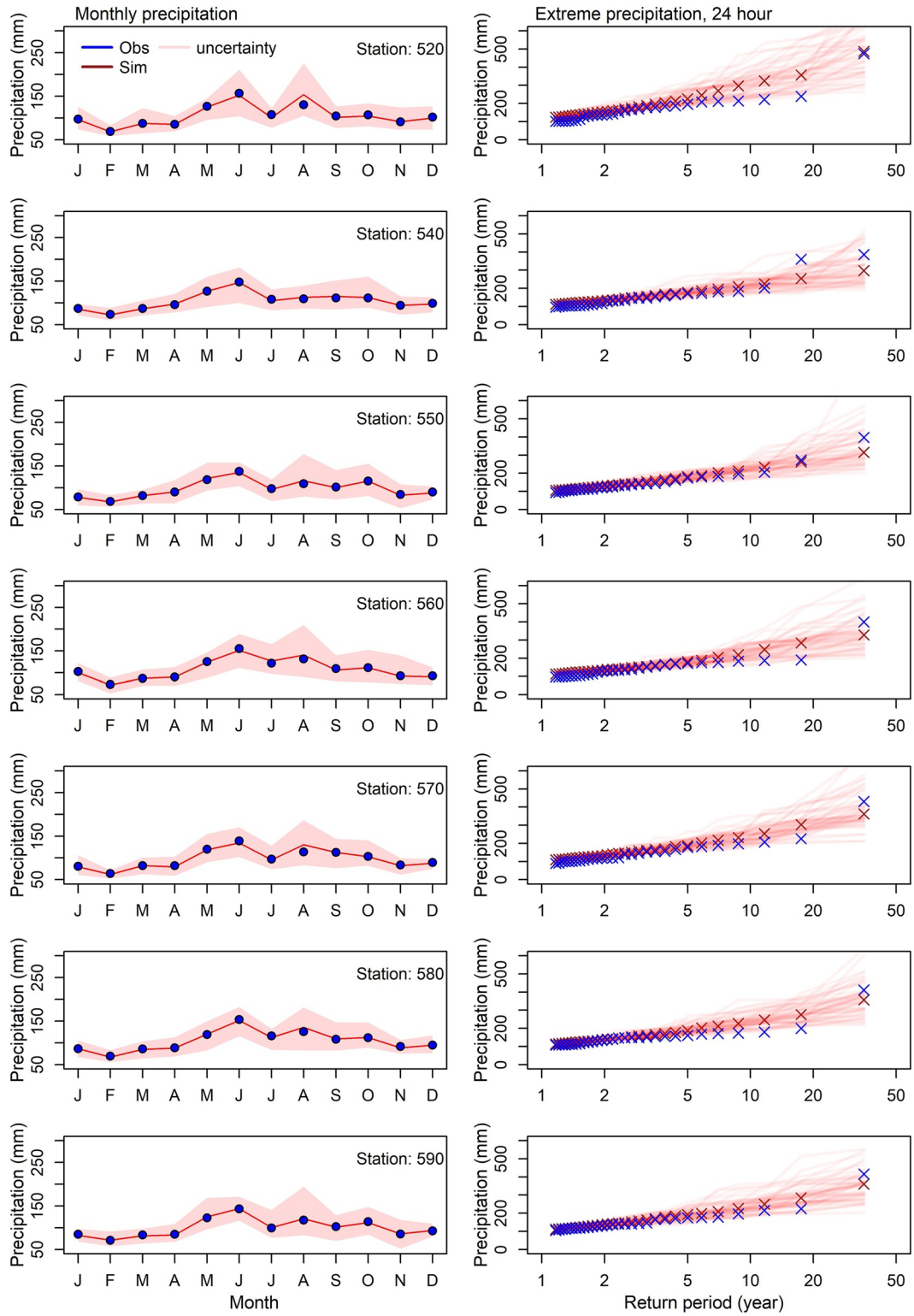

Figure 6. Comparison of mean monthly precipitation and extreme precipitation of 24-hr duration from observations and Advanced WEather GENerator (AWE-GEN) model simulations for historical (1986–2020) period. *Red* line (left) and marker (right) denote the median and shaded region denotes 95% uncertainty limits of 50 AWE-GEN simulations denoting stochastic uncertainty from internal climate variability.

relatively wider uncertainty range for the month of August in monthly precipitation estimates. Nonetheless, the downscaling methodology adopted in this study computes the stochastic uncertainty in future simulation, therefore reliable inferences can be made on future changes of extreme precipitation. The AWE-GEN model shows similar performance for hourly simulations at all stations thus improving its reliability in simulations of future changes (Figure S14 in Supporting Information S2).

4.4.2. BWA-Based Factors of Change

FCs for future climate are derived from the realizations of GCMs for control and future periods. In this study, we use GCM outputs at the grid cell closest to White Oak Bayou watershed for all stations because the spatial extent of watershed (~310 km^2) is very small relative to the extent of GCM grid cell. Fatichi et al. (2011) examined the sensitivity of GCM outputs with respect to a given location and found that GCM realizations for a given model are spatially self-consistent. In other words, the difference in change factors for a given GCM along neighboring cells is very small in comparison to the difference among different models for the same location. Therefore, GCM outputs at a single grid cell can be taken as representative for a small area enclosed within. Out of initially considered 15 GCMs listed in Table S1 in Supporting Information S3, the five best performing models are selected using the scatterplot (Figure S15 in Supporting Information S2) of Model RMSE Index (MRI) versus Model PBIAS Index (MPI) index for extreme precipitation indices from 15 GCMs (Table S2 in Supporting Information S3). Finally selected five GCMs are—HadGEM3-GC31-LL, IPSL-CM6A-LR, CNRM-ESM2-1, EC-Earth3, and EC-Earth3-Veg.

We compute the posterior distribution of FC for 170 distinct statistics of temperature and precipitation used in AWE-GEN model using BWA approach. Figure 7 illustrates the product FCs for mean monthly precipitation computed from individual GCMs and 95% quantile range of posterior distribution of FC for station 520. As can be seen, FC for monthly precipitation from individual GCMs exhibits large variability with values ranging from 0.3 to 2.2 in different months. The variability of FC is relatively larger for SSP5-8.5 and SSP1-2.6 than SSP2-4.5. The uncertainty in FC from individual GCMs considerably reduces in pdf of FC obtained from BWA (Figure 7). In all scenarios, the value of FC in the pdf is larger than 1 in spring and early summer (March-June) suggesting an increase, and less than 1 for summer and early autumn (July-September) suggesting a reduction in future precipitation. For the remaining months, FCs are distributed around unity indicating no definite change. Similarly, pdfs of FCs are obtained for 169 other statistics of temperature and precipitation for two future periods and three future scenarios at each station. An example posterior distribution of FC for mean temperature and precipitation for August month is shown in Figure S16 in Supporting Information S2.

4.4.3. Future Hourly Precipitation

We sampled 51 sets of FCs from the posterior pdfs and each set of FCs is applied to the parameters of AWE-GEN model setup for historical period to get a new set of model parameter representing a trajectory in future climate. With each new set of AWE-GEN model parameters, 50 simulations are performed to generate an ensemble of 30-year long hourly time series of meteorological parameters. Figure 8 shows the distribution of design extreme precipitation estimated by fitting stationary GEV model to each stochastic simulation of hourly precipitation for median future trajectory. For station 520 (Figure 8a), the comparison of observations with median of distribution for future period shows a consistent reduction in design extreme precipitation for all selected return periods in near future period (2021–2050). In addition, the reduction in design precipitation is found in all three future scenarios. In the far future (2071–2100) period, however, we obtain varying results for different scenarios—the median of projected design precipitation shows considerable decline in SSP2-4.5, a minor reduction in SSP5-8.5, and no observable change in SSP1-2.6. As evident from Figure 8b, we obtain similar results for projected extreme precipitation at all other stations in White Oak Bayou. Overall, extreme precipitation shows considerable reduction in the near future in all three future scenarios at all stations. Whereas design extreme precipitation in the far future period exhibits consistent reduction in SSP2-4.5 scenario, and minor changes in other two scenarios with an increase at few stations and decline at others. The ensemble of AWE-GEN model simulations also gives a wide range of uncertainty about the median in which quantile range above median is much wider than the quantile range below median. The upper quantile limit for future estimates is considerably larger (1.2–2 times) than the observational design precipitation. It suggests that the future design precipitation is fairly likely to exceed the observational estimates by a large magnitude, particularly in high future emission scenario. Interestingly, monthly precipitation shows marginal change in future periods in three scenarios. The median monthly precipitation for future periods is fairly close to the observed monthly precipitation (Figure S17 in Supporting Information S2).

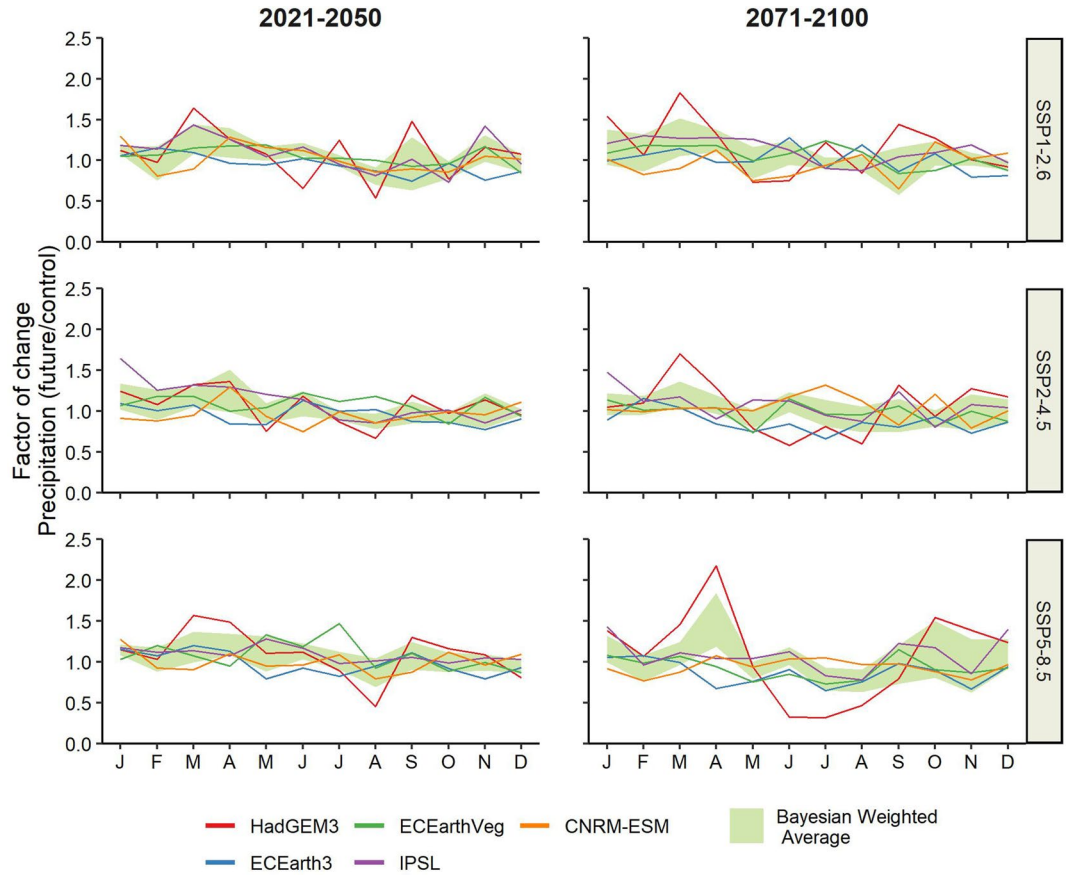

Figure 7. Product factor of change (FC) for mean monthly 24-hr precipitation from individual general circulation models (GCMs) and 95% quantile bound of posterior pdf of FC estimated using Bayesian weighted average of GCMs. Product FC is computed as ratio of general circulation model simulated mean precipitation for future (2021–2050 and 2071–2100) and control (1986–2014) period for selected three future scenarios (SSP1-2.6, SSP2-4.5., SSP5-8.5).

4.5. Uncertainty in Design Precipitation

In future design precipitation the uncertainty from climate models and stochastic uncertainty are computed to ascertain their relative contribution and dominance in total uncertainty. Figure 9 shows the distribution of percent contribution of the two uncertainty sources in total uncertainty in design precipitation for selected durations and return period at station 520. Evidently, future design precipitation is dominated by stochastic uncertainty that accounts to approximately 50%–100% of total uncertainty, whereas contribution of climate model uncertainty varies in the range 30%–70%, approximately (Figure 9a). The fractional contribution of stochastic uncertainty in design precipitation increases in the far (2071–2100) future period than the near (2021–2050) future period. Figure 9b shows the distribution of relative magnitude of stochastic and climate model uncertainty computed as their ratio. In the figure, relative magnitude for majority of future design precipitation events is distributed above unity which shows a higher magnitude of stochastic uncertainty than climate model uncertainty for majority of extreme events. The magnitude of stochastic uncertainty is 1.5–2.5 times larger than the magnitude of climate model uncertainty for most future events in the near future, that further rises to 2–3 fold in the far future period. Similar results are obtained for all other stations in White Oak Bayou watershed. It shows that the uncertainty induced from the use of multiple GCMs is considerably smaller than the stochastic uncertainty emerging from natural variability of regional climate. Figure 9c shows the distribution of the ratio of total uncertainty in future design precipitation to historical design precipitation. Evidently, total uncertainty in future and historical design precipitation is comparable in the near (2021–2050) future period as the median is close to unity. However, uncertainty in future design precipitation is larger than that in historical estimates in the far (2071–2100) future period.

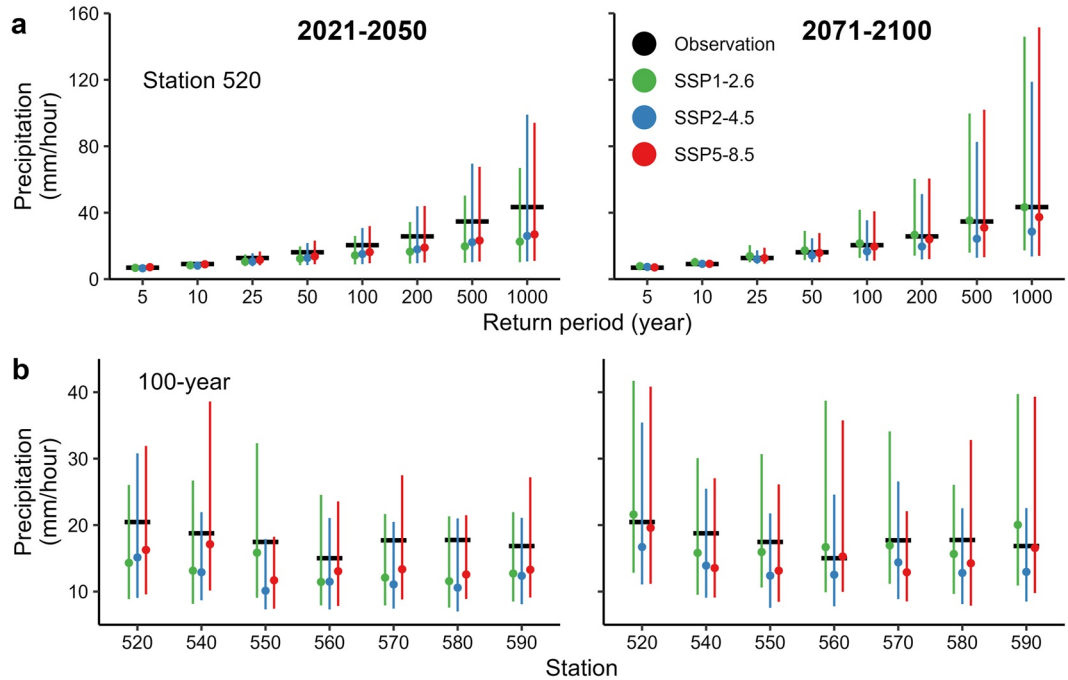

Figure 8. Design extreme precipitation of 24-hr aggregation from observations and 50 stochastic simulations of Advanced WEather GENerator for median future trajectory for two (2021–2050 and 2071–2100) future periods in three (SSP1-2.6, SSP2-4.5, and SSP5-8.5) future emission scenarios. Future projections of precipitation are compared with the observations (bar, *black*). Median future trajectory corresponds to median of pdf of factor of change in a given future scenario. Point represents the median of values from stochastic simulations and range gives the 95% uncertainty limits. Comparison of 24-hr design extreme precipitation from observations and two future (2021–2050 and 2071–2100) periods (a) at station 520 for all selected return periods (b) at all stations in White Oak Bayou for 100-year return period.

4.6. Simulated Flood Response

To achieve the equilibrium of mass balance in the ICPR model, model simulations are generated for 48 hr (two days) before the design storm of 24-hr duration. To investigate the nature and magnitude of difference in flood response to design storm for historical and future period, we compare the peak streamflow corresponding to 24-hr 100-year design storm (Figure S18 in Supporting Information S2). Comparison of simulated streamflow for design storm of future period in three emission scenarios is shown in Figure 10. Consistent with the results for design extreme precipitation, for SSP1-2.6 and SSP2-4.5 scenario, simulated streamflow in the far future (2071–2100) is higher than the streamflow for the near future (2021–2050). The peak streamflow in 2071–2100

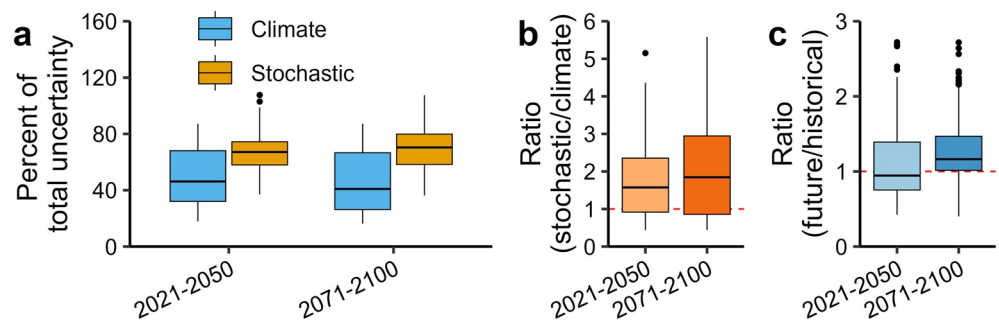

Figure 9. Relative contribution of uncertainty from climate model and internal climate variability (stochastic uncertainty) to total uncertainty in future design precipitation for two (2021–2050 and 2071–2100) future periods. (a) Distribution of percent contribution from two sources for design precipitation of selected durations and return periods. (b) Distribution of the ratio of stochastic to climate model uncertainty for selected duration and return period events. (c) Distribution of ratio of uncertainty in future and historical design precipitation.

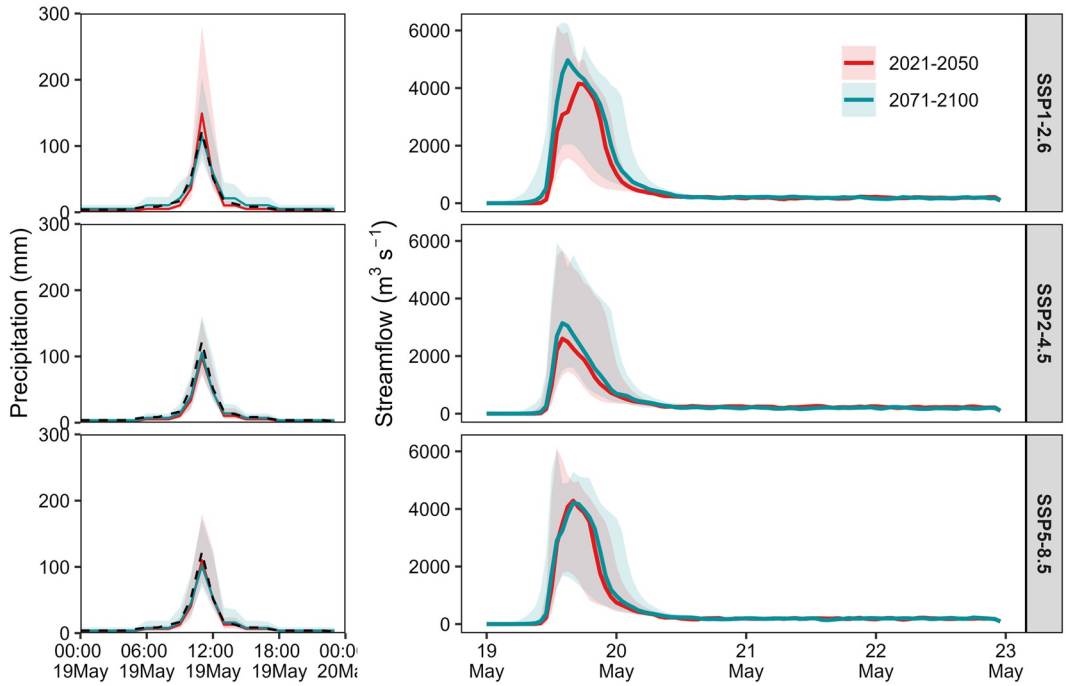

Figure 10. Interconnected Channel and Pond Routing simulated streamflow hydrograph corresponding to 24-hr 100-year design storm for two future periods (2021–2050 and 2071–2100) in three emission scenarios (SSP1-2.6, SSP2-4.5, and SSP5-8.5).

is ∼19% and ∼11% higher than 2021–2050 in SSP1-2.6 and SSP2-4.5 scenarios, respectively. On the other hand, simulated streamflow for SSP5-8.5 scenarios is comparable in both future periods. These results indicate that the difference in design precipitation for future periods is evident in simulated streamflow from the urban flood model, especially in low and moderate emission scenarios.

5. Discussion and Conclusions

This study proposes a comprehensive framework for fine-scale assessment of urban flood response to changing climate. The influence of climate change is accounted for through modeling the changes in extreme precipitation in historical observations as well as future projections. We demonstrate the proposed framework on a highly urbanized watershed of White Oak Bayou in Houston, Texas considering a historical period (1986–2020) and two future periods (2021–2050 and 2071–2100) in three emission scenarios (SSP1-2.6, SSP2-4.5, and SSP5-8.5). Nonstationary modeling of extreme precipitation in historical period gives significantly higher design precipitation estimates than the stationary models at all stations in White Oak Bayou watershed. It is mainly due to a significant increasing trend of extreme precipitation in observed records. In White Oak Bayou, the difference in design precipitation from nonstationary versus stationary models is especially prominent (up to 35%–40%) for longer duration (>12-hr) and smaller return period (<200-year) events. These results suggest that the assumption of stationary extreme precipitation as used in, for example, NOAA Atlas 14, may not be valid for the Houston region. Consequently, a direct use of NOAA's design precipitation estimates in infrastructure design or flood mitigation planning for this region would involve considerable risk. For the White oak Bayou watershed, we recommend correction factors to NOAA's precipitation estimates for different return periods (or exceedance probabilities) corresponding to 24-hr duration precipitation as listed in Table S10 in Supporting Information S3. It may be used by Harris County Flood Control District for different analysis and infrastructural design.

On the contrary, future extreme precipitation for White Oak Bayou exhibits a considerable decline in both the future periods in all scenarios. Results show that the design precipitation for median future trajectory is consistently less than the observational design precipitation in all three emission scenarios. Although, among two future periods, the decline is larger in near future (2021–2050) than far future (2071–2100) period, and among three scenarios, decline is smaller in SSP8-4.5 scenario. These results are in contrast to the widely reported increase in

extreme precipitation from future GCM projections for different parts of the world including the US (Donat et al., 2016; Easterling et al., 2017; IPCC, 2014; Scoccimarro et al., 2013). The contrasting patterns for the study region are possibly due to the limited performance of GCMs in resolving small-scale (synoptic to meso-scale) weather processes owing to the course spatial resolution of existing GCMs (Feng et al., 2021; Ridder et al., 2021; Villarini et al., 2014; Wehner et al., 2015). Extreme precipitation events along the southern and eastern coasts of the US are largely associated with such small-scale weather systems, such as tropical cyclones (Khouakhi et al., 2017; J. A. Smith et al., 2011; Villarini et al., 2014). Therefore, GCM projections show limited capability in providing a correct representation of extreme precipitation response to future climate in the region.

These contrasting results for historical and future period indicate that flood response assessment in the study area with only the consideration of future projected changes in precipitation from GCMs may lead to erroneous conclusions. Such discrepancy in observed and future projected changes in extreme precipitation may exist for other parts of the world, particularly in the regions where extreme precipitation dynamics is dominated by small scale phenomena and local factors. Therefore, collective assessment with the consideration of changes in both historical observations and future projections is necessary for reliable decision making and planning. A collective assessment is also crucial to ascertain whether flood response to historical changes envelopes the flood response to future projected changes in extreme precipitation and vice-versa. The framework proposed in the present study would serve as an efficient tool for such a holistic assessment of urban floods in changing climate, that can be used for other major cities with confidence.

With the proposed framework, we attempt to answer two important research questions. Whether the difference in design precipitation from nonstationary versus stationary modeling is reflected in flood simulations? Yes. Distributed urban flood models are characterized with considerable inherent complexities from model structure and parameterization that can suppress minor changes in input meteorological variables (Y. Liu & Gupta, 2007; Merwade et al., 2008; Wang et al., 2018). Also, external factors such as LULC change, flow control structures, and infrastructure development may alter sensitivity of system response (e.g., streamflow) to inputs (e.g., precipitation and temperature) (Gangrade et al., 2018). Past studies report that while extreme precipitation exhibits significant trends in larger parts of the US, observed streamflow show no significant change at most gauging sites (A. Sharma et al., 2018). In this study, we find that model simulated streamflow for nonstationary design precipitation is substantially higher than that for stationary estimates in terms of peak flow and total flow volume. It shows that the difference in stationary versus nonstationarity based design precipitation are substantial to cause significant change in hydrologic response of White Oak Bayou watershed. Considerably higher streamflow response for nonstationary design precipitation highlights the risk associated with the assumption of stationary extreme precipitation for the study region.

In the second question, we examine which source of uncertainty dominates the design precipitation estimates obtained by incorporating the changing climate. Stochastic uncertainty dominates the future design precipitation. Stochastic uncertainty represents the uncertainty due to natural variability in the local climate, thus is irreducible. Its dominance in total uncertainty involved with future design precipitation narrows down the possibility of reduction of uncertainty in local-scale precipitation projections even with future improvements in climate model structure and emission scenarios. Nonetheless, the distinct signal of climate change evident from median future trajectory should be taken into consideration for future planning. The dominance of stochastic uncertainty highlights the importance of its comprehensive evaluation along with climate model uncertainty in future projections of regional climate variables. Although, it will continue to restrict the communication of precise information on local precipitation changes in future climate. In addition, large uncertainty in future design precipitation also suggests that the commonly used approach in climate change impact studies that consider one or a few deterministic climate projections (Ali & Mishra, 2018; Seager et al., 2007), could be misleading especially in regards to interpretation and communication of precise conclusions for practical applications. Study results also show that total uncertainty in future precipitation is comparable with the uncertainty in historical design precipitation in the near future period, whereas, higher in the far future period. Thus, concentrated efforts are needed for improvement in methods for modeling of changes in extremes to reduce the uncertainty in nonstationary modeling of historical design precipitation.

As previously mentioned, White Oak Bayou watershed is characterized by cyclonic activities-driven extreme precipitation, saturation level of urbanization, and flatter terrain. These attributes are common to multiple major cities around the world, especially located along the coastlines in tropical and subtropical climates. In addition, most of the prominent

cities are either approaching or projecting toward a saturation level of urbanization. Thus, White Oak Bayou watershed can be considered a "bellwether" watershed for similar urban agglomerations. Accordingly, the conclusion from the present study that significant change in extreme precipitation due to nonstationarity consideration has resulted in a significant change in flood response can be extended for such urbanized catchments. However, some of the findings from the case study may not be generalized for other similar catchments because of the regional heterogeneity in climate patterns and geophysical characteristics of the catchment. We suggest that distinctive analysis should be performed for an urban watershed of interest to assess the impacts of climate change on flood response. The framework proposed in the present study would certainly facilitate such analysis by providing a collective assessment of historical as well as future changes in precipitation and robust estimates of associated uncertainties.

While the proposed framework fills multiple critical gaps in the existing literature and show potential for application in urban flood assessment and decision making, there still exists a few limitations suggesting potential avenues of improvement and future research.

- The proposed framework does not account for uncertainty from hydrodynamic flood modeling. Thus, caution should be taken in interpreting the results in reference to other potential sources. Past studies show that the relative contribution of uncertainty from hydrodynamic modeling in climate change impact assessment depends on several factors including, catchment properties, selection of hydrodynamic model, and selected hydrologic indicator (Meresa et al., 2021; Steinschneider et al., 2015; Velázquez et al., 2013). We recommend an adequate evaluation of the uncertainty from hydrodynamic model together with the uncertainty estimates given by the present framework for robust assessment and reliable communication of the findings. Literature contains efficient methods for evaluation of uncertainty in distributed flood modeling (Bates et al., 2014; Z. Liu & Merwade, 2018, 2019). In future work, our efforts will be concentrated on developing a fully Bayesian approach-based framework for comprehensive uncertainty estimation from different sources in urban flood assessment in changing climate.
- We used two-dimensional distributed ICPR model for flood simulations with a conventional assumption of impervious surface. This assumption may not provide realistic estimates of flood inundation. A recent study shows that 2-D hydrodynamic surface water model overpredicts the peak and underpredicts the low flows (Saksena et al., 2019). Thus, for detailed and more accurate applications such as, analysis of inundation extent and time of inundation, users are advised to use an integrated hydrodynamic model with surface and sub-surface processes. Nonetheless, the current model structure serves satisfactorily for the aims of this study primarily for two reasons—first, we are interested in evaluation of relative response of the system that is, stationary versus nonstationary and stationary versus future changes; second, the study region is 96% urbanized with more than 60% impervious land cover that closely validates the assumption of impervious surface in model structure.
- The present methodology uses future climate projections from GCMs that are typically efficient in simulating large-scale atmosphere-ocean processes. Urban climate, however, is affected by multiple local urbanization effects such as, urban heat island, urban canopy layer, and varying aerosol concentration. These factors can potentially affect the precipitation climatology of flood events (Huong & Pathirana, 2013). Alternatively, a meso-scale regional climate model such as Weather Research and Forecasting model can be used to assess dynamic response of local climatology to the influence of urbanization as well as for spatiotemporal downscaling of GCM (Patel et al., 2019, 2020). RCMs are also capable of simulating meso-scale processes such as tropical cyclones, thus may provide accurate response of associated extreme precipitation to future climate (K. Emanuel et al., 2008; K. A. Emanuel, 2013).
- We assume LULC to be unchanged in flood simulations for future periods based on the fact that 96% of the watershed is urban land cover in 2019, thus the watershed is almost at saturation level of urbanization. The LULC change in the future would be minor over the study region, if at all, that justifies our assumption. However, adequate consideration of possible future LULC in the assessment is recommended in application to cities with high LULC change potential.
- We selected five GCMs for future projections that may not include the entire range of climate model uncertainty. More climate models can be included to cover a wider range of information on future climate projections for better evaluation of climate model uncertainty.
- In nonstationary modeling of historical extreme precipitation, GEV distribution parameters can be scaled on the covariates using a non-linear model for improved assessment of change in extremes.
- The stochastic downscaling procedure used in the proposed framework requires higher computational resources that may be realized in application to a larger domain with larger number of rainfall gauging sites.

With the aforementioned scope of improvements, the demonstration of proposed framework in the case study reveals its capability in providing critical insights on the influence of climate change on regional extreme precipitation characteristics and the response of urban floods to these changes. The framework is designed to make use of the entire available knowledge on change in climate through the consideration of historical as well as future periods. Thus, the framework would help in robust evaluation of flood risk and potential flood damage in the backdrop of climate change. A potential application of the proposed framework can be envisaged in the revision of NOAA's design precipitation estimates to incorporate nonstationarity in extreme precipitation with the consideration of regional heterogeneity in local or large-scale drivers of nonstationarity. The framework would also be beneficial in re-evaluation of FEMA's flood inundation maps with the consideration of changing extreme precipitation patterns. We envisage several potential applications of the framework including, identification of flood risk hotspots and vulnerability assessment, re-evaluation of flood inundation maps and subsequent assessment of expected losses for insurance industries, revaluation of efficiency, stability of flood protection structure, etc.

Appendix A: Mathematical Description

A1. Stationary Generalized Extreme Value (GEV) Distribution

The GEV distribution represents the theoretical asymptotic distribution of block maxima. For $x_1, x_2, \ldots, x_n$ be a sequence of n independent and identically distributed random variables denoting annual maximum series, the cumulative distribution function of GEV distribution is given by (Coles, 2001):

$$\mathrm{GEV}(x;\,\mu,\sigma,\xi)=\begin{cases}\exp\left\{-\left[1+\frac{\xi(x-\mu)}{\sigma}\right]^{-1/\xi}\right\}, 1+\xi(x-\mu)/\sigma>0, \xi\neq 0\\ \exp\left\{-\exp\left[-\frac{x-\mu}{\sigma}\right]\right\}, \xi=0\end{cases} \tag{A1}$$

where μ, $\sigma>0$, and ξ are location, scale and shape parameters, respectively. The distribution is characterized as heavy tailed $\mu-\sigma/\xi<x<\infty$ for $\xi>0$, unbound light tailed $-\infty\leq x\leq\infty$ for $\xi=0$, and bounded upper tailed $-\infty<x<\mu-\sigma/\xi$ for $\xi<0$.

The estimates of the GEV distribution parameters are obtained using the method of maximum likelihood. The log-likelihood function for the above distribution can be derived as (Beirlant et al., 2004; Coles, 2001):

$$\begin{aligned}\log L(\mu,\sigma,\xi|X)=&-n\log\sigma-(1+1/\xi)\sum_{i=1}^{n}\log\left[1+\xi\left(\frac{x_i-\mu}{\sigma}\right)\right]\\&-\sum_{i=1}^{n}\left[1+\xi\left(\frac{x_i-\mu}{\sigma}\right)\right]^{-1/\xi},\xi\neq 0, 1+\xi\left(\frac{x_i-\mu}{\sigma}\right)>0\end{aligned} \tag{A2}$$

$$\log L(\mu,\sigma|X)=-n\log\sigma-\sum_{i=1}^{n}\left(\frac{x_i-\mu}{\sigma}\right)-\sum_{i=1}^{n}\exp\left[-\left(\frac{x_i-\mu}{\sigma}\right)\right],\xi=0 \tag{A3}$$

For the ease of computation, the negative log-likelihood $-\log L(\theta|X);\theta=\{\mu,\sigma,\xi\}$ is minimized to obtain the parameter estimates. The model parameter estimates are then used to compute the rainfall intensity (or return level) for a given probability of exceedance, p as (Agilan & Umamahesh, 2018; Coles, 2001):

$$Z_T=\begin{cases}\hat{\mu}+\frac{\hat{\sigma}}{\hat{\xi}}\left[(-\log(1-p))^{-\hat{\xi}}-1\right], & \hat{\xi}\neq 0\\ \hat{\mu}+\hat{\sigma}[-\log(-\log(1-p))], & \hat{\xi}=0\end{cases} \tag{A4}$$

The probability of exceedance (p) is linked to the return period (T) of a rainfall event as $T=1/p$. In other words, "T" year rainfall event represents that intensity of annual maximum rainfall of a given duration that has $1/T$ probability of exceeding in a given year (L. Cheng & AghaKouchak, 2014).

A2. Selection of Best-Fit Candidate Nonstationary GEV Model

The best-fit nonstationary GEV model is identified using three criteria—Akaike Information Criteria (AIC), Bayesian Information Criteria (BIC), and Likelihood Ratio (LR) test. The AIC and BIC values for a given model is given by

$$\mathrm{AIC} = -2\log L(\theta|X) + 2p \tag{A5a}$$

$$\mathrm{BIC} = -2\log L(\theta|X) + p\log(n) \tag{A5b}$$

where p is the number of parameters of the model. The model with minimum value for AIC and BIC represents the most significant covariate.

The statistical significance of best-fit nonstationary model can be checked by testing a null hypothesis of no trend (stationary model). The test can be performed by comparing the minimized negative log-likelihood function for two given models. For θ_0 and θ_1 be the parameters of the two models under comparison, then the deviance statistics (D) is given by (Coles, 2001):

$$D(\theta_1) = 2\left[\log L(\theta_0) - \log L(\theta_1)\right] \tag{A6}$$

Under suitable regularity conditions and large n, the deviance statistics approximately follows a chi-square distribution ($D(\theta_1) \sim \chi^2$) with the degree of freedom equal to the difference between the number of parameters of the two models. The significance of model-fit is tested at 5% significance level in the present study.

A3. Selection of GCMs

Following the approach used by Srivastava et al. (2020), Extreme Precipitation Indices defined by the Expert Team on Climate Change (ETCCDI) are analyzed for GCM's historical and observed precipitation for control period (See Table S2 in Supporting Information S3). The performance of GCMs is evaluated using two measures—Normalized Root Mean Squared Error (NRMSE) and Normalized Percent Bias (NPBIAS) given as (Akinsanola et al., 2021; Srivastava et al., 2020):

$$\mathrm{NRMSE}_{m,i} = \frac{\mathrm{RMSE}_{m,i} - \mathrm{med}\left(\mathrm{RMSE}_{\mathrm{cmip6},i}\right)}{\mathrm{med}\left(\mathrm{RMSE}_{\mathrm{cmip6},i}\right)} \tag{A7a}$$

$$\mathrm{NPBIAS}_{m,i} = \frac{\mathrm{abs}(\mathrm{PBIAS}_{m,i}) - \mathrm{med}\left(\mathrm{abs}\left(\mathrm{PBIAS}_{\mathrm{cmip6},i}\right)\right)}{\mathrm{med}\left(\mathrm{abs}\left(\mathrm{PBIAS}_{\mathrm{cmip6},i}\right)\right)} \tag{A7b}$$

where $\mathrm{med}(\mathrm{RMSE}_{\mathrm{cmip6},i})$ denotes the median of RMSE across all the considered CMIP6 GCMs for a given index i, and

$$\mathrm{RMSE}_{m,i} = \left[\frac{1}{N}\sum_{n=1}^{N}(s_n - o_n)^2\right]^{1/2} \tag{A8}$$

$$\mathrm{PBIAS}_{m,i} = \frac{\sum_{n=1}^{N}(s_n - o_n)}{\sum_{n=1}^{N} o_n} \times 100 \tag{A9}$$

for a given model m, computed over N observations. Here, s_n and o_n represent GCM simulated, and station observed value of index for a given year n. The accumulated performance of a GCM over all extreme indices is evaluated by a median of NRMSE and NPBIAS namely Model RMSE Index (MRI) and Model PBIAS Index (MPI). The top five GCM are selected based on the overall performance evaluated through a scatterplot of MRI versus MPI. The lesser the value of MRI and MPI, better the model performance in simulating extreme precipitation.

Data Availability Statement

All data used in the study are publicly available. The precipitation data used in the study are retrieved from Harris County Flood Warning System at https://www.harriscountyfws.org/Document_Library. NOAA's precipitation frequency estimates are obtained from Precipitation Frequency Data Server (PFDS) of NOAA at https://hdsc.nws.noaa.gov/pfds/. River discharge and stage data set is obtained from the US Geological Survey National Water Information System at https://waterdata.usgs.gov/nwis. Meteorological data are downloaded from NOAA's

National Centers for Environmental Information (NCEI) at https://www.ncei.noaa.gov/. Solar radiation data set is acquired from National Solar Radiation Database (Marion & Urban, 1995; Wilcox, 2012) provided by National Renewable Energy Laboratory at https://nsrdb.nrel.gov/data-sets/archives. Land cover and impervious cover data set is available from USGS's National Landcover Database 2019 (Dewitz & US Geological Survey, 2021) at https://doi.org/10.5066/P9KZCM54. Gridded Soil Survey Geographic (gSSURGO) data set (Soil Survey Staff, 2017) provided by US Department of Agriculture Natural Resources Conservation Service is downloaded from https://gdg.sc.egov.usda.gov/. SST index for Niño 3.4 is obtained from Working Group on Surface Pressure of NOAA's Physical Sciences Laboratory at http://psl.noaa.gov/gcos_wgsp/Timeseries/Nino34/index.html. Hadley Centre Sea Ice and Sea Surface Temperature (Version 2.1) (HadISST2) (Titchner & Rayner, 2014) from Met Office Hadley Centre observations can be downloaded at https://www.metoffice.gov.uk/hadobs/hadisst/. Precipitation and temperature projections from GCMs under CMIP6 (Eyring et al., 2016) are downloaded from https://esgf-node.llnl.gov/search/cmip6/. All data processing, statistical analysis and visualization are performed in R environment (R Core Team, 2021). Statistical modelling of extreme precipitation is performed using extRemes v2.1-1 (Gilleland & Katz, 2016) package licensed under GPL-3. The MATLAB source code of AWE-GEN (Ivanov et al., 2007) model with a sample data can be downloaded at http://www-personal.umich.edu/~ivanov/HYDROWIT/Models.html.

Acknowledgments
This work is output of the research done during Lalit Pal's visit to Purdue University under the SERB-Purdue University Overseas Visiting Doctoral Fellowship program funded by Science and Engineering Research Board (SERB), Government of India (File No.-SB/S9/Z-03/2017-XIII (2019–2020)). This work was partially supported by the National Oceanic and Atmospheric Administration (NOAA) through the Adaptation Science Program on the project titled, "Identification of Cost-Effective, Climate-Informed Green Infrastructure Adaptations to Reduce Flood Risk in Houston's Vulnerable Communities" (Project NA21OAR4310270) and the "Urban Flooding Open Knowledge Network" (Project 2033607) supported by the National Science Foundation (NSF). Any opinions, findings, conclusions, or recommendations expressed in this material are those of the authors and do not necessarily reflect the views of the funding agencies. Authors thank Dr. Simone Fatichi, National University of Singapore for providing the MATLAB codes for AWE-GEN weather generator-based downscaling.

References

Adhikari, P., Hong, Y., Douglas, K. R., Kirschbaum, D. B., Gourley, J., Adler, R., & Brakenridge, G. R. (2010). A digitized global flood inventory (1998-2008): Compilation and preliminary results. *Natural Hazards*, *55*(2), 405–422. https://doi.org/10.1007/S11069-010-9537-2/FIGURES/12

Agel, L., & Barlow, M. (2020). How well do CMIP6 historical runs match observed Northeast U.S. precipitation and extreme precipitation–related circulation? *Journal of Climate*, *33*(22), 9835–9848. https://doi.org/10.1175/JCLI-D-19-1025.1

Agilan, V., & Umamahesh, N. V. (2018). Covariate and parameter uncertainty in non-stationary rainfall IDF curve. *International Journal of Climatology*, *38*(1), 365–383. https://doi.org/10.1002/joc.5181

Ahmad, H., Miller, J. W., & George, R. D. (2014). Minimizing pond size using an off-site pond in a closed basin: A storm flow mitigation design and evaluation. *International Journal of Sustainable Development and Planning*, *9*(2), 211–224. https://doi.org/10.2495/SDP-V9-N2-211-224

Akinsanola, A. A., Ongoma, V., & Kooperman, G. J. (2021). Evaluation of CMIP6 models in simulating the statistics of extreme precipitation over Eastern Africa. *Atmospheric Research*, *254*, 105509. https://doi.org/10.1016/J.ATMOSRES.2021.105509

Alexander, L. V., Zhang, X., Peterson, T. C., Caesar, J., Gleason, B., Klein Tank, A. M. G., et al. (2006). Global observed changes in daily climate extremes of temperature and precipitation. *Journal of Geophysical Research*, *111*(D5), D05109. https://doi.org/10.1029/2005JD006290

Ali, H., & Mishra, V. (2018). Increase in subdaily precipitation extremes in India under 1.5 and 2.0°C warming worlds. *Geophysical Research Letters*, *45*(14), 6972–6982. https://doi.org/10.1029/2018GL078689

Allen, M. R., & Ingram, W. J. (2002). Constraints on future changes in climate and the hydrologic cycle. *Nature*, *419*(6903), 228–232. https://doi.org/10.1038/nature01092

Asadieh, B., & Krakauer, N. Y. (2015). Global trends in extreme precipitation: Climate models versus observations. *Hydrology and Earth System Sciences*, *19*(2), 877–891. https://doi.org/10.5194/HESS-19-877-2015

Ashley, S. T., & Ashley, W. S. (2008). Flood fatalities in the United States. *Journal of Applied Meteorology and Climatology*, *47*(3), 805–818. https://doi.org/10.1175/2007JAMC1611.1

Ban, N., Caillaud, C., Coppola, E., Pichelli, E., Sobolowski, S., Adinolfi, M., et al. (2021). The first multi-model ensemble of regional climate simulations at kilometer-scale resolution, part I: Evaluation of precipitation. *Climate Dynamics*, *57*(1), 275–302. https://doi.org/10.1007/S00382-021-05708-W/FIGURES/11

Bates, P. D., & De Roo, A. P. J. (2000). A simple raster-based model for flood inundation simulation. *Journal of Hydrology*, *236*(1), 54–77. https://doi.org/10.1016/S0022-1694(00)00278-X

Bates, P. D., Pappenberger, F., & Romanowicz, R. J. (2014). Uncertainty in flood inundation modelling. In *Applied uncertainty analysis for flood risk management* (pp. 232–269).

Bates, P. D., Quinn, N., Sampson, C., Smith, A., Wing, O., Sosa, J., et al. (2021). Combined modeling of US fluvial, pluvial, and coastal flood hazard under current and future climates. *Water Resources Research*, *57*(2), e2020WR028673. https://doi.org/10.1029/2020WR028673

Beirlant, J., Goegebeur, Y., Segers, J., & Teugels, J. L. (2004). Statistics of extremes: Theory and applications.

Berndtsson, R., Becker, P., Persson, A., Aspegren, H., Haghighatafshar, S., Jönsson, K., et al. (2019). Drivers of changing urban flood risk: A framework for action. *Journal of Environmental Management*, *240*, 47–56. https://doi.org/10.1016/J.JENVMAN.2019.03.094

Brunner, G. W. (2016). HEC-RAS River Analysis System: Hydraulic Reference Manual, Version 5.0.

Cheng, C., Yang, Y. C. E., Ryan, R., Yu, Q., & Brabec, E. (2017). Assessing climate change-induced flooding mitigation for adaptation in Boston's Charles River watershed, USA. *Landscape and Urban Planning*, *167*, 25–36. https://doi.org/10.1016/J.LANDURBPLAN.2017.05.019

Cheng, L., & AghaKouchak, A. (2014). Nonstationary precipitation intensity-duration-frequency curves for infrastructure design in a changing climate. *Scientific Reports*, *4*(1), 7093. https://doi.org/10.1038/srep07093

Chou, C., Neelin, J. D., Chen, C. A., & Tu, J. Y. (2009). Evaluating the "rich-get-richer" mechanism in tropical precipitation change under global warming. *Journal of Climate*, *22*(8), 1982–2005. https://doi.org/10.1175/2008JCLI2471.1

Chow, V. T., Maidment, D. R., & Mays, L. W. (1988). *Applied hydrology*. McGraw-Hill.

Coles, S. (2001). *An introduction to statistical modeling of extreme values*. Springer London. https://doi.org/10.1007/978-1-4471-3675-0

Collet, L., Beevers, L., & Stewart, M. D. (2018). Decision-making and flood risk uncertainty: Statistical data set analysis for flood risk assessment. *Water Resources Research*, *54*(10), 7291–7308. https://doi.org/10.1029/2017WR022024

Das, T., Maurer, E. P., Pierce, D. W., Dettinger, M. D., & Cayan, D. R. (2013). Increases in flood magnitudes in California under warming climates. *Journal of Hydrology*, *501*, 101–110. https://doi.org/10.1016/J.JHYDROL.2013.07.042

DeFlorio, M. J., Pierce, D. W., Cayan, D. R., & Miller, A. J. (2013). Western U.S. extreme precipitation events and their relation to ENSO and PDO in CCSM4. *Journal of Climate*, *26*(12), 4231–4243. https://doi.org/10.1175/JCLI-D-12-00257.1

Devanand, A., Huang, M., Ashfaq, M., Barik, B., & Ghosh, S. (2019). Choice of irrigation water management practice affects Indian summer monsoon rainfall and its extremes. *Geophysical Research Letters*, *46*(15), 9126–9135. https://doi.org/10.1029/2019GL083875

Dewitz, J., & US Geological Survey. (2021). National Land Cover Database (NLCD) 2019 products (ver. 2.0, June 2021) [Dataset]. U.S. Geological Survey data release. https://doi.org/10.5066/P9KZCM54

Dickey, D. A., & Fuller, W. A. (1979). Distribution of the estimators for autoregressive time series with a unit root. *Journal of the American Statistical Association*, *74*(366), 427–431. https://doi.org/10.1080/01621459.1979.10482531

Donat, M. G., Alexander, L. V., Yang, H., Durre, I., Vose, R., Dunn, R. J. H., et al. (2013). Updated analyses of temperature and precipitation extreme indices since the beginning of the twentieth century: The HadEX2 dataset. *Journal of Geophysical Research: Atmospheres*, *118*(5), 2098–2118. https://doi.org/10.1002/JGRD.50150

Donat, M. G., Lowry, A. L., Alexander, L. V., O'Gorman, P. A., & Maher, N. (2016). More extreme precipitation in the world's dry and wet regions. *Nature Climate Change*, *6*(5), 508–513. https://doi.org/10.1038/nclimate2941

Dritsakis, N. (2004). Tourism as a long-run economic growth factor: An empirical investigation for Greece using causality analysis. *Tourism Economics*, *10*(3), 305–316. https://doi.org/10.5367/0000000041895094

Du, H., Alexander, L. V., Donat, M. G., Lippmann, T., Srivastava, A., Salinger, J., et al. (2019). Precipitation from persistent extremes is increasing in most regions and globally. *Geophysical Research Letters*, *46*(11), 6041–6049. https://doi.org/10.1029/2019GL081898

Easterling, D. R., Kunkel, K. E., Arnold, J. R., Knutson, T., LeGrande, A. N., Leung, L. R., et al. (2017). Precipitation change in the United States. In D. J. Wuebbles, D. W. Fahey, K. A. Hibbard, D. J. Dokken, B. C. Stewart, & T. K. Maycock (Eds.), *Climate Science Special Report: Fourth National Climate Assessment* (Vol. I, pp. 207–230). U.S. Global Change Research Program. https://doi.org/10.7930/J0H993CC

Egger, C., & Maurer, M. (2015). Importance of anthropogenic climate impact, sampling error and urban development in sewer system design. *Water Research*, *73*, 78–97. https://doi.org/10.1016/J.WATRES.2014.12.050

Emanuel, K., Sundararajan, R., & Williams, J. (2008). Hurricanes and global warming: Results from downscaling IPCC AR4 simulations. *Bulletin of the American Meteorological Society*, *89*(3), 347–368. https://doi.org/10.1175/BAMS-89-3-347

Emanuel, K. A. (2013). Downscaling CMIP5 climate models shows increased tropical cyclone activity over the 21st century. *Proceedings of the National Academy of Sciences*, *110*(30), 12219–12224. https://doi.org/10.1073/pnas.1301293110

Enfield, D. B., Mestas-Nuñez, A. M., Mayer, D. A., & Cid-Serrano, L. (1999). How ubiquitous is the dipole relationship in tropical Atlantic sea surface temperatures? *Journal of Geophysical Research*, *104*(C4), 7841–7848. https://doi.org/10.1029/1998JC900109

Eyring, V., Bony, S., Meehl, G. A., Senior, C. A., Stevens, B., Stouffer, R. J., & Taylor, K. E. (2016). Overview of the Coupled Model Intercomparison Project Phase 6 (CMIP6) experimental design and organization. *Geoscientific Model Development*, *9*(5), 1937–1958. https://doi.org/10.5194/gmd-9-1937-2016

Fatichi, S., Ivanov, V. Y., & Caporali, E. (2011). Simulation of future climate scenarios with a weather generator. *Advances in Water Resources*, *34*(4), 448–467. https://doi.org/10.1016/J.ADVWATRES.2010.12.013

Fatichi, S., Ivanov, V. Y., & Caporali, E. (2013). Assessment of a stochastic downscaling methodology in generating an ensemble of hourly future climate time series. *Climate Dynamics*, *40*(7), 1841–1861. https://doi.org/10.1007/S00382-012-1627-2/FIGURES/11

Fatichi, S., Ivanov, V. Y., Paschalis, A., Peleg, N., Molnar, P., Rimkus, S., et al. (2016). Uncertainty partition challenges the predictability of vital details of climate change. *Earth's Future*, *4*(5), 240–251. https://doi.org/10.1002/2015EF000336

Federal Emergency Management Agency (FEMA). (2022). FEMA floods & maps. Retrieved from https://www.fema.gov/flood-maps/guidance-reports/guidelines-standards/technical-references-flood-risk-analysis-and-mapping

Feng, Z., Song, F., Sakaguchi, K., & Leung, L. R. (2021). Evaluation of mesoscale convective systems in climate simulations: Methodological development and results from MPAS-CAM over the United States. *Journal of Climate*, *34*(7), 2611–2633. https://doi.org/10.1175/JCLI-D-20-0136.1

Fischer, E. M., & Knutti, R. (2015). Anthropogenic contribution to global occurrence of heavy-precipitation and high-temperature extremes. *Nature Climate Change*, *5*(6), 560–564. https://doi.org/10.1038/nclimate2617

Gangrade, S., Kao, S.-C., Naz, B. S., Rastogi, D., Ashfaq, M., Singh, N., & Preston, B. L. (2018). Sensitivity of probable maximum flood in a changing environment. *Water Resources Research*, *54*(6), 3913–3936. https://doi.org/10.1029/2017WR021987

Ganguli, P., & Coulibaly, P. (2017). Does nonstationarity in rainfall require nonstationary intensity-duration-frequency curves? *Hydrology and Earth System Sciences*, *21*(12), 6461–6483. https://doi.org/10.5194/HESS-21-6461-2017

Gilleland, E. (2020). Bootstrap methods for statistical inference. Part II: Extreme-value analysis. *Journal of Atmospheric and Oceanic Technology*, *37*(11), 2135–2144. https://doi.org/10.1175/JTECH-D-20-0070.1

Gilleland, E., & Katz, R. W. (2016). extRemes 2.0: An extreme value analysis package in R [Software]. Journal of Statistical Software, *72*(8), 1–39. https://doi.org/10.18637/jss.v072.i08

Gimeno, R., Manchado, B., & Mínguez, R. (1999). Stationarity tests for financial time series. *Physica A: Statistical Mechanics and its Applications*, *269*(1), 72–78. https://doi.org/10.1016/S0378-4371(99)00081-3

Groisman, P. Y., Knight, R. W., & Karl, T. R. (2001). Heavy precipitation and high streamflow in the contiguous United States: Trends in the twentieth century. *Bulletin of the American Meteorological Society*, *82*(2), 219–246. https://doi.org/10.1175/1520-0477(2001)082<0219:HPAHSI>2.3.CO;2

Guzman, O., & Jiang, H. (2021). Global increase in tropical cyclone rain rate. *Nature Communications*, *12*(1), 5344. https://doi.org/10.1038/s41467-021-25685-2

Hallegatte, S., Green, C., Nicholls, R. J., & Corfee-Morlot, J. (2013). Future flood losses in major coastal cities. *Nature Climate Change*, *3*(9), 802–806. https://doi.org/10.1038/nclimate1979

Hamed, K. H., & Ramachandra Rao, A. (1998). A modified Mann-Kendall trend test for autocorrelated data. *Journal of Hydrology*, *204*(1–4), 182–196. https://doi.org/10.1016/S0022-1694(97)00125-X

Hirabayashi, Y., Mahendran, R., Koirala, S., Konoshima, L., Yamazaki, D., Watanabe, S., et al. (2013). Global flood risk under climate change. *Nature Climate Change*, *3*(9), 816–821. https://doi.org/10.1038/nclimate1911

Hofstra, N., Haylock, M., New, M., Jones, P., & Frei, C. (2008). Comparison of six methods for the interpolation of daily, European climate data. *Journal of Geophysical Research*, *113*(D21), D21110. https://doi.org/10.1029/2008JD010100

Huang, H., Winter, J. M., & Osterberg, E. C. (2018). Mechanisms of abrupt extreme precipitation change over the Northeastern United States. *Journal of Geophysical Research: Atmospheres*, *123*(14), 7179–7192. https://doi.org/10.1029/2017JD028136

Huong, H. T. L., & Pathirana, A. (2013). Urbanization and climate change impacts on future urban flooding in Can Tho city, Vietnam. *Hydrology and Earth System Sciences*, *17*(1), 379–394. https://doi.org/10.5194/hess-17-379-2013

Hutchinson, M. F., & Gessler, P. E. (1994). Splines—More than just a smooth interpolator. *Geoderma*, *62*(1–3), 45–67. https://doi.org/10.1016/0016-7061(94)90027-2

IPCC. (2014). In R. K., Pachauri, & L., Meyer (Eds.), *Climate Change 2014: Synthesis report. Contribution of Working Groups I, II and III to the Fifth Assessment Report of the Intergovernmental Panel on Climate Change*. IPCC. Retrieved from https://epic.awi.de/id/eprint/37530/1/IPCC_AR5_SYR_Final.pdf

Ivanov, V. Y., Bras, R. L., & Curtis, D. C. (2007). A weather generator for hydrological, ecological, and agricultural applications. *Water Resources Research*, *43*(10), W10406. https://doi.org/10.1029/2006WR005364

Janssen, E., Wuebbles, D. J., Kunkel, K. E., Olsen, S. C., & Goodman, A. (2014). Observational- and model-based trends and projections of extreme precipitation over the contiguous United States. *Earth's Future*, *2*(2), 99–113. https://doi.org/10.1002/2013EF000185

Joyce, J., Chang, N.-B., Harji, R., Ruppert, T., & Singhofen, P. (2018). Cascade impact of hurricane movement, storm tidal surge, sea level rise and precipitation variability on flood assessment in a coastal urban watershed. *Climate Dynamics*, *51*(1), 383–409. https://doi.org/10.1007/s00382-017-3930-4

Karamouz, M., Asce, F., Forough, & Zahmatkesh, Z. (2017). Distributed hydrologic modeling of coastal flood inundation and damage: Nonstationary approach. *Journal of Irrigation and Drainage Engineering*, *143*(8), 04017019. https://doi.org/10.1061/(ASCE)IR.1943-4774.0001173

Katz, R. W. (2013). Statistical methods for nonstationary extremes. In A. AghaKouchak, D. Easterling, K. Hsu, S. Schubert, & S. Sorooshian (Eds.), *Extremes in a changing climate: Detection, analysis and uncertainty* (pp. 15–37). Springer Netherlands. https://doi.org/10.1007/978-94-007-4479-0_2

Kendall, M. G. (1970). *Rank correlation methods*. Charles Griffin.

Kenyon, J., & Hegerl, G. C. (2010). Influence of modes of climate variability on global precipitation extremes. *Journal of Climate*, *23*(23), 6248–6262. https://doi.org/10.1175/2010JCLI3617.1

Khouakhi, A., Villarini, G., & Vecchi, G. A. (2017). Contribution of tropical cyclones to rainfall at the global scale. *Journal of Climate*, *30*(1), 359–372. https://doi.org/10.1175/JCLI-D-16-0298.1

Kim, J., Ivanov, V. Y., & Fatichi, S. (2016). Climate change and uncertainty assessment over a hydroclimatic transect of Michigan. *Stochastic Environmental Research and Risk Assessment*, *30*(3), 923–944. https://doi.org/10.1007/S00477-015-1097-2/FIGURES/9

Knutson, T. R., McBride, J. L., Chan, J., Emanuel, K., Holland, G., Landsea, C., et al. (2010). Tropical cyclones and climate change. *Nature Geoscience*, *3*(3), 157–163. https://doi.org/10.1038/ngeo779

Knutson, T. R., Sirutis, J. J., Vecchi, G. A., Garner, S., Zhao, M., Kim, H.-S., et al. (2013). Dynamical downscaling projections of twenty-first-century Atlantic hurricane activity: CMIP3 and CMIP5 model-based scenarios. *Journal of Climate*, *26*(17), 6591–6617. https://doi.org/10.1175/JCLI-D-12-00539.1

Kourtis, I. M., & Tsihrintzis, V. A. (2021). Adaptation of urban drainage networks to climate change: A review. *Science of the Total Environment*, *771*, 145431. https://doi.org/10.1016/J.SCITOTENV.2021.145431

Kunkel, K. E., Easterling, D. R., Kristovich, D. A. R., Gleason, B., Stoecker, L., Smith, R., et al. (2010). Recent increases in U.S. heavy precipitation associated with tropical cyclones. *Geophysical Research Letters*, *37*(24), L24706. https://doi.org/10.1029/2010GL045164

Kwiatkowski, D., Phillips, P. C. B., Schmidt, P., & Shin, Y. (1992). Testing the null hypothesis of stationarity against the alternative of a unit root: How sure are we that economic time series have a unit root? *Journal of Econometrics*, *54*(1–3), 159–178. https://doi.org/10.1016/0304-4076(92)90104-Y

Liu, Y., & Gupta, H. V. (2007). Uncertainty in hydrologic modeling: Toward an integrated data assimilation framework. *Water Resources Research*, *43*(7). https://doi.org/10.1029/2006WR005756

Liu, Z., & Merwade, V. (2018). Accounting for model structure, parameter and input forcing uncertainty in flood inundation modeling using Bayesian model averaging. *Journal of Hydrology*, *565*, 138–149. https://doi.org/10.1016/J.JHYDROL.2018.08.009

Liu, Z., & Merwade, V. (2019). Separation and prioritization of uncertainty sources in a raster based flood inundation model using hierarchical Bayesian model averaging. *Journal of Hydrology*, *578*, 124100. https://doi.org/10.1016/j.jhydrol.2019.124100

Mann, H. B. (1945). Nonparametric tests against trend. *Econometrica*, *13*(3), 245–259. https://doi.org/10.2307/1907187

Marion, W., & Urban, K. (1995). User's manual for TMY2s (typical meteorological years)-derived from the 1961-1990 National Solar Radiation Data Base (No. NREL/TP-463-7668) [Dataset]. National Renewable Energy Laboratory (NREL). Retrieved from https://www.nrel.gov/docs/legosti/old/4859.pdf

Mattos, T. S., Oliveira, P. T. S., de Souza Bruno, L., de Oliveira, N. D., Vasconcelos, J. G., & Lucas, M. C. (2021). Improving urban flood resilience under climate change scenarios in a tropical watershed using low-impact development practices. *Journal of Hydrologic Engineering*, *26*(12), 5021031. https://doi.org/10.1061/(ASCE)HE.1943-5584.0002143

Meresa, H., Murphy, C., Fealy, R., & Golian, S. (2021). Uncertainties and their interaction in flood hazard assessment with climate change. *Hydrology and Earth System Sciences*, *25*(9), 5237–5257. https://doi.org/10.5194/hess-25-5237-2021

Merwade, V., Olivera, F., Arabi, M., & Edleman, S. (2008). Uncertainty in flood inundation mapping: Current issues and future directions. *Journal of Hydrologic Engineering*, *13*(7), 608–620. https://doi.org/10.1061/(ASCE)1084-0699(2008)13:7(608)

Milly, P. C. D., Betancourt, J., Falkenmark, M., Hirsch, R. M., Kundzewicz, Z. W., Lettenmaier, D. P., & Stouffer, R. J. (2008). Climate change: Stationarity is dead: Whither water management? *Science*, *319*(5863), 573–574. https://doi.org/10.1126/SCIENCE.1151915/ASSET/194346FF-04E7-4E18-97C5-3F8B61E450AE/ASSETS/GRAPHIC/573-2.GIF

Mondal, A., & Mujumdar, P. P. (2015). Modeling non-stationarity in intensity, duration and frequency of extreme rainfall over India. *Journal of Hydrology*, *521*, 217–231. https://doi.org/10.1016/J.JHYDROL.2014.11.071

O'Donnell, E. C., & Thorne, C. R. (2020). Drivers of future urban flood risk. *Philosophical Transactions of the Royal Society A*, *378*(2168), 378. https://doi.org/10.1098/RSTA.2019.0216

Padulano, R., Rianna, G., Costabile, P., Costanzo, C., Del Giudice, G., & Mercogliano, P. (2021). Propagation of variability in climate projections within urban flood modelling: A multi-purpose impact analysis. *Journal of Hydrology*, *602*, 126756. https://doi.org/10.1016/J.JHYDROL.2021.126756

Patel, P., Ghosh, S., Kaginalkar, A., Islam, S., & Karmakar, S. (2019). Performance evaluation of WRF for extreme flood forecasts in a coastal urban environment. *Atmospheric Research*, *223*, 39–48. https://doi.org/10.1016/j.atmosres.2019.03.005

Patel, P., Karmakar, S., Ghosh, S., & Niyogi, D. (2020). Improved simulation of very heavy rainfall events by incorporating WUDAPT urban land use/land cover in WRF. *Urban Climate*, *32*, 100616. https://doi.org/10.1016/j.uclim.2020.100616

Patricola, C. M., & Wehner, M. F. (2018). Anthropogenic influences on major tropical cyclone events. *Nature*, *563*(7731), 339–346. https://doi.org/10.1038/s41586-018-0673-2

Perica, S., Pavlovic, S., St. Laurent, M., Trypaluk, C., Unruh, D., & Wilhite, O. (2018). In N. W. S. United States (Ed.), *Precipitation-frequency Atlas of the United States. Volume 11, version 2.0. Texas*. https://doi.org/10.25923/1ceg-5094

Phillips, P. C. B., & Perron, P. (1988). Testing for a unit root in time series regression. *Biometrika*, *75*(2), 335–346. https://doi.org/10.1093/BIOMET/75.2.335

Rappaport, E. N. (2014). Fatalities in the United States from Atlantic tropical cyclones: New data and interpretation. *Bulletin of the American Meteorological Society*, *95*(3), 341–346. https://doi.org/10.1175/BAMS-D-12-00074.1

R Core Team. (2021). R: A language and environment for statistical computing [Software]. Retrieved from https://www.r-project.org/

Reidmiller, D. R., Avery, C. W., Easterling, D. R., Kunkel, K. E., Lewis, K. L., Maycock, T. K., & Stewart, B. C. (2017). Impacts, risks, and adaptation in the United States: Fourth National Climate Assessment, volume II.

Riahi, K., van Vuuren, D. P., Kriegler, E., Edmonds, J., O'Neill, B. C., Fujimori, S., et al. (2017). The Shared Socioeconomic Pathways and their energy, land use, and greenhouse gas emissions implications: An overview. *Global Environmental Change*, *42*, 153–168. https://doi.org/10.1016/J.GLOENVCHA.2016.05.009

Ridder, N. N., Pitman, A. J., & Ukkola, A. M. (2021). Do CMIP6 climate models simulate global or regional compound events skillfully? *Geophysical Research Letters*, *48*(2), e2020GL091152. https://doi.org/10.1029/2020GL091152

Said, S. E., & Dickey, D. A. (1984). Testing for unit roots in autoregressive-moving average models of unknown order. *Biometrika*, *71*(3), 599–607. https://doi.org/10.1093/BIOMET/71.3.599

Saksena, S., Dey, S., Merwade, V., & Singhofen, P. J. (2020). A computationally efficient and physically based approach for urban flood modeling using a flexible spatiotemporal structure. *Water Resources Research*, *56*(1), e2019WR025769. https://doi.org/10.1029/2019WR025769

Saksena, S., Merwade, V., & Singhofen, P. J. (2019). Flood inundation modeling and mapping by integrating surface and subsurface hydrology with river hydrodynamics. *Journal of Hydrology*, *575*, 1155–1177. https://doi.org/10.1016/j.jhydrol.2019.06.024

Saltelli, A., Chan, K., & Scott, E. M. (2009). In *Sensitivity analysis*. In *Probability and statistics series*. John Wiley and Sons.

Sanders, B. F., Schubert, J. E., Goodrich, K. A., Houston, D., Feldman, D. L., Basolo, V., et al. (2020). Collaborative modeling with fine-resolution data enhances flood awareness, minimizes differences in flood perception, and produces actionable flood maps. *Earth's Future*, *8*(1), e2019EF001391. https://doi.org/10.1029/2019EF001391

Scoccimarro, E., Gualdi, S., Bellucci, A., Zampieri, M., & Navarra, A. (2013). Heavy precipitation events in a warmer climate: Results from CMIP5 models. *Journal of Climate*, *26*(20), 7902–7911. https://doi.org/10.1175/JCLI-D-12-00850.1

Scoccimarro, E., Gualdi, S., Villarini, G., Vecchi, G. A., Zhao, M., Walsh, K., & Navarra, A. (2014). Intense precipitation events associated with landfalling tropical cyclones in response to a warmer climate and increased CO_2. *Journal of Climate*, *27*(12), 4642–4654. https://doi.org/10.1175/JCLI-D-14-00065.1

Seager, R., Ting, M., Held, I., Kushnir, Y., Lu, J., Vecchi, G., et al. (2007). Model projections of an imminent transition to a more arid climate in southwestern North America. *Science*, *316*(5828), 1181–1184. https://doi.org/10.1126/science.1139601

Sharma, A., Wasko, C., & Lettenmaier, D. P. (2018). If precipitation extremes are increasing, why aren't floods? *Water Resources Research*, *54*(11), 8545–8551. https://doi.org/10.1029/2018WR023749

Sharma, S., Gomez, M., Keller, K., Nicholas, R. E., & Mejia, A. (2021). Regional flood risk projections under climate change. *Journal of Hydrometeorology*, *22*(9), 2259–2274. https://doi.org/10.1175/JHM-D-20-0238.1

Sillmann, J., Pozzoli, L., Vignati, E., Kloster, S., & Feichter, J. (2013). Aerosol effect on climate extremes in Europe under different future scenarios. *Geophysical Research Letters*, *40*(10), 2290–2295. https://doi.org/10.1002/GRL.50459

Singh, J., Karmakar, S., Paimazumder, D., Ghosh, S., & Niyogi, D. (2020). Urbanization alters rainfall extremes over the contiguous United States. *Environmental Research Letters*, *15*(7), 074033. https://doi.org/10.1088/1748-9326/AB8980

Smith, J. A., Villarini, G., & Baeck, M. L. (2011). Mixture distributions and the hydroclimatology of extreme rainfall and flooding in the eastern United States. *Journal of Hydrometeorology*, *12*(2), 294–309. https://doi.org/10.1175/2010JHM1242.1

Smith, R. L., Tebaldi, C., Nychka, D., & Mearns, L. O. (2009). Bayesian modeling of uncertainty in ensembles of climate models. *Journal of the American Statistical Association*, *104*(485), 97–116. https://doi.org/10.1198/jasa.2009.0007

Sobel, A. H., Camargo, S. J., Hall, T. M., Lee, C. Y., Tippett, M. K., & Wing, A. A. (2016). Human influence on tropical cyclone intensity. *Science*, *353*(6296), 242–246. https://doi.org/10.1126/SCIENCE.AAF6574/SUPPL_FILE/AAF6574-SOBEL-SM.PDF

Sobol, I. M. (1976). Uniformly distributed sequences with an additional uniform property. *USSR Computational Mathematics and Mathematical Physics*, *16*(5), 236–242. https://doi.org/10.1016/0041-5553(76)90154-3

Soil Survey Staff. (2017). Gridded Soil Survey Geographic (gSSURGO) Database for Texas [Dataset]. Retrieved from https://gdg.sc.egov.usda.gov/

Srivastava, A., Grotjahn, R., & Ullrich, P. A. (2020). Evaluation of historical CMIP6 model simulations of extreme precipitation over contiguous US regions. *Weather and Climate Extremes*, *29*, 100268. https://doi.org/10.1016/J.WACE.2020.100268

Steinschneider, S., Wi, S., & Brown, C. (2015). The integrated effects of climate and hydrologic uncertainty on future flood risk assessments. *Hydrological Processes*, *29*(12), 2823–2839. https://doi.org/10.1002/hyp.10409

Streamline Technologies. (2016). ICPR4 validation report. Retrieved from www.streamnologies.com/misc/ICPR4_DOCS.zip

Streamline Technologies. (2018). ICPR4 technical reference manual. Retrieved from www.streamnologies.com/misc/ICPR4_DOCS.zip

Szentimrey, T., Bihari, Z., & Szalai, S. (2007). Comparison of geostatistical and meteorological interpolation methods (what is what?). In *Spatial interpolation for climate data* (pp. 45–56). https://doi.org/10.1002/9780470612262.ch4

Tebaldi, C., Smith, R. L., Nychka, D., & Mearns, L. O. (2005). Quantifying uncertainty in projections of regional climate change: A Bayesian approach to the analysis of multimodel ensembles. *Journal of Climate*, *18*(10), 1524–1540. https://doi.org/10.1175/JCLI3363.1

Titchner, H. A., & Rayner, N. A. (2014). The Met Office Hadley Centre Sea Ice and sea surface temperature data set, version 2: 1. Sea ice concentrations. *Journal of Geophysical Research: Atmospheres*, *119*(6), 2864–2889. https://doi.org/10.1002/2013JD020316

Tousi, E. G., O'Brien, W., Doulabian, S., & Toosi, A. S. (2021). Climate changes impact on stormwater infrastructure design in Tucson Arizona. *Sustainable Cities and Society*, *72*, 103014. https://doi.org/10.1016/j.scs.2021.103014

Trenberth, K. E., Dai, A., Rasmussen, R. M., & Parsons, D. B. (2003). The changing character of precipitation. *Bulletin of the American Meteorological Society*, *84*(9), 1205–1218. https://doi.org/10.1175/BAMS-84-9-1205

Underwood, B. S., Asce, A. M., Mascaro, G., Chester, M. V., Fraser, A., Lopez-Cantu, T., et al. (2020). Past and present design practices and uncertainty in climate projections are challenges for designing infrastructure to future conditions. *Journal of Infrastructure Systems*, *26*(3), 04020026. https://doi.org/10.1061/(ASCE)IS.1943-555X.0000567

Van Der Wiel, K., Kapnick, S. B., Jan Van Oldenborgh, G., Whan, K., Philip, S., Vecchi, G. A., et al. (2017). Rapid attribution of the August 2016 flood-inducing extreme precipitation in south Louisiana to climate change. *Hydrology and Earth System Sciences*, *21*(2), 897–921. https://doi.org/10.5194/HESS-21-897-2017

Van Oldenborgh, G. J., Van Der Wiel, K., Sebastian, A., Singh, R., Arrighi, J., Otto, F., et al. (2017). Attribution of extreme rainfall from Hurricane Harvey. *Environmental Research Letters*, *12*(12), 124009. https://doi.org/10.1088/1748-9326/AA9EF2

Velázquez, J. A., Schmid, J., Ricard, S., Muerth, M. J., Gauvin St-Denis, B., Minville, M., et al. (2013). An ensemble approach to assess hydrological models' contribution to uncertainties in the analysis of climate change impact on water resources. *Hydrology and Earth System Sciences*, *17*(2), 565–578. https://doi.org/10.5194/hess-17-565-2013

Vemula, S., Raju, K. S., Veena, S. S., & Kumar, A. S. (2019). Urban floods in Hyderabad, India, under present and future rainfall scenarios: A case study. *Natural Hazards*, *95*(3), 637–655. https://doi.org/10.1007/S11069-018-3511-9/FIGURES/9

Villarini, G., Goska, R., Smith, J. A., & Vecchi, G. A. (2014). North Atlantic tropical cyclones and U.S. flooding. *Bulletin of the American Meteorological Society*, *95*(9), 1381–1388. https://doi.org/10.1175/BAMS-D-13-00060.1

Villarini, G., Smith, J. A., Serinaldi, F., Bales, J., Bates, P. D., & Krajewski, W. F. (2009). Flood frequency analysis for nonstationary annual peak records in an urban drainage basin. *Advances in Water Resources*, *32*(8), 1255–1266. https://doi.org/10.1016/J.ADVWATRES.2009.05.003

Villarini, G., Smith, J. A., & Vecchi, G. A. (2013). Changing frequency of heavy rainfall over the Central United States. *Journal of Climate*, *26*(1), 351–357. https://doi.org/10.1175/JCLI-D-12-00043.1

Vu, T. M., & Mishra, A. K. (2019). Nonstationary frequency analysis of the recent extreme precipitation events in the United States. *Journal of Hydrology*, *575*, 999–1010. https://doi.org/10.1016/J.JHYDROL.2019.05.090

Wallemacq, P., Guha-Sapir, D., & McClean, D. (2015). The human Cost of weather related disasters (1995-2015). Retrieved from http://www.unisdr.org/2015/docs/climatechange/COP21_WeatherDisastersReport_2015_FINAL.pdf

Wang, Y., Chen, A. S., Fu, G., Djordjević, S., Zhang, C., & Savić, D. A. (2018). An integrated framework for high-resolution urban flood modelling considering multiple information sources and urban features. *Environmental Modelling & Software*, *107*, 85–95. https://doi.org/10.1016/j.envsoft.2018.06.010

Webster, P. J., Holland, G. J., Curry, J. A., & Chang, H. R. (2005). Changes in tropical cyclone number, duration, and intensity in a warming environment. *Science*, *309*(5742), 1844–1846. https://doi.org/10.1126/SCIENCE.1116448/ASSET/EC277365-85DA-4321-B704-FE0F487B21F5/ASSETS/GRAPHIC/309_1844_F4.JPEG

Wehner, M., Prabhat Reed, K. A., Stone, D., Collins, W. D., & Bacmeister, J. (2015). Resolution dependence of future tropical cyclone projections of CAM5.1 in the U.S. CLIVAR Hurricane Working Group idealized configurations. *Journal of Climate*, *28*(10), 3905–3925. https://doi.org/10.1175/JCLI-D-14-00311.1

Westra, S., Alexander, L. V., & Zwiers, F. W. (2013). Global increasing trends in annual maximum daily precipitation. *Journal of Climate*, *26*(11), 3904–3918. https://doi.org/10.1175/JCLI-D-12-00502.1

Wilcox, S. M. (2012). National Solar Radiation Database 1991-2010 update: User's manual (No. NREL/TP-5500-54824) [Dataset]. National Renewable Energy Laboratory (NREL). Retrieved from https://www.nrel.gov/docs/fy12osti/54824.pdf

Wing, O. E. J., Bates, P. D., Smith, A. M., Sampson, C. C., Johnson, K. A., Fargione, J., & Morefield, P. (2018). Estimates of present and future flood risk in the conterminous United States. *Environmental Research Letters*, *13*(3), 034023. https://doi.org/10.1088/1748-9326/AAAC65

Winsemius, H. C., Aerts, J. C. J. H., Van Beek, L. P. H., Bierkens, M. F. P., Bouwman, A., Jongman, B., et al. (2016). Global drivers of future river flood risk. *Nature Climate Change*, *6*(4), 381–385. https://doi.org/10.1038/nclimate2893

Wright, D. B., Bosma, C. D., & Lopez-Cantu, T. (2019). U.S. hydrologic design standards insufficient due to large increases in frequency of rainfall extremes. *Geophysical Research Letters*, *46*(14), 8144–8153. https://doi.org/10.1029/2019GL083235

Wright, D. B., Knutson, T. R., & Smith, J. A. (2015). Regional climate model projections of rainfall from U.S. landfalling tropical cyclones. *Climate Dynamics*, *45*(11), 3365–3379. https://doi.org/10.1007/S00382-015-2544-Y/FIGURES/8

Yazdanfar, Z., & Sharma, A. (2015). Urban drainage system planning and design – Challenges with climate change and urbanization: A review. *Water Science and Technology*, *72*(2), 165–179. https://doi.org/10.2166/WST.2015.207

Zahmatkesh, Z., Karamouz, M., Mohammad Asce, F., Goharian, E., Asce, S. M., Burian, S. J., & Asce, M. (2015). Analysis of the effects of climate change on urban storm water runoff using statistically downscaled precipitation data and a change factor approach. *Journal of Hydrologic Engineering*, *20*(7), 05014022. https://doi.org/10.1061/(ASCE)HE.1943-5584.0001064

Zhang, W., Villarini, G., Vecchi, G. A., & Smith, J. A. (2018). Urbanization exacerbated the rainfall and flooding caused by Hurricane Harvey in Houston. *Nature*, *563*(7731), 384–388. https://doi.org/10.1038/s41586-018-0676-z

Zhang, X., Wang, J., Zwiers, F. W., & Groisman, P. Y. (2010). The influence of large-scale climate variability on winter maximum daily precipitation over North America. *Journal of Climate*, *23*(11), 2902–2915. https://doi.org/10.1175/2010JCLI3249.1

Zhao, A. D., Stevenson, D. S., & Bollasina, M. A. (2019). The role of anthropogenic aerosols in future precipitation extremes over the Asian Monsoon Region. *Climate Dynamics*, *52*(9), 6257–6278. https://doi.org/10.1007/S00382-018-4514-7/FIGURES/3